

University of Denver

Digital Commons @ DU

Electronic Theses and Dissertations

Graduate Studies

8-1-2018

Ice Adhesion Analysis of Severely Aged PDMS Rubbers

Theodore R. Woll
University of Denver

Follow this and additional works at: <https://digitalcommons.du.edu/etd>



Part of the [Engineering Science and Materials Commons](#)

Recommended Citation

Woll, Theodore R., "Ice Adhesion Analysis of Severely Aged PDMS Rubbers" (2018). *Electronic Theses and Dissertations*. 1504.

<https://digitalcommons.du.edu/etd/1504>

This Thesis is brought to you for free and open access by the Graduate Studies at Digital Commons @ DU. It has been accepted for inclusion in Electronic Theses and Dissertations by an authorized administrator of Digital Commons @ DU. For more information, please contact jennifer.cox@du.edu, dig-commons@du.edu.

Ice Adhesion Analysis of Severely Aged PDMS Rubbers

Abstract

The goal of this study was to evaluate and optimize the ice adhesion test initially developed by the University of Denver and to examine Polydimethylsiloxane (PDMS) based silicone rubbers for their ice-phobicity as a function of their physical and chemistry properties, and under severe oxidative aging. The test is based on an ice block bonded to a silicone rubber substrate and subjected to shear. In its original state, the test had severe limitations that caused the ice to be dislodged through a mixture of shear and peeling. Several steps were taken in this research to improve the test, and the work was successfully supported by finite element numerical simulations. Testing PDMS rubber substrates of various crosslink densities revealed that their ice adhesion strengths decreased as the crosslinking was reduced. It was shown for the first time that aging in hypochlorous acid greatly affected ice-phobicity of the rubbers.

Document Type

Thesis

Degree Name

M.S.

Department

Materials Science

First Advisor

Maciej Kumosa, Ph.D.

Second Advisor

Susan Sadler, Ph.D.

Third Advisor

Matt Gordon

Keywords

Accelerated aging, Icephobic, Ice shedding, Polydimethylsiloxane

Subject Categories

Engineering | Engineering Science and Materials

Publication Statement

Copyright is held by the author. User is responsible for all copyright compliance.

ICE ADHESION ANALYSIS OF SEVERELY AGED PDMS RUBBERS

A Thesis

Presented to

the Faculty of the Daniel Felix Ritchie School of Engineering and Computer Science

University of Denver

In Partial Fulfillment

of the Requirements for the Degree

Master of Science

by

Theodore R. Woll

August 2018

Advisor: Dr. Maciej Kumosa

Author: Theodore R. Woll

Title: ICE ADHESION ANALYSIS OF SEVERELY AGED PDMS RUBBERS

Advisor: Dr. Maciej Kumosa

Degree Date: August 2018

Abstract

The goal of this study was to evaluate and optimize the ice adhesion test initially developed by the University of Denver and to examine Polydimethylsiloxane (PDMS) based silicone rubbers for their ice-phobicity as a function of their physical and chemistry properties, and under severe oxidative aging. The test is based on an ice block bonded to a silicone rubber substrate and subjected to shear. In its original state, the test had severe limitations that caused the ice to be dislodged through a mixture of shear and peeling. Several steps were taken in this research to improve the test, and the work was successfully supported by finite element numerical simulations. Testing PDMS rubber substrates of various crosslink densities revealed that their ice adhesion strengths decreased as the crosslinking was reduced. It was shown for the first time that aging in hypochlorous acid greatly affected ice-phobicity of the rubbers.

Acknowledgements

Thanks to my advisor, Dr. Maciej Kumosa, for his support and Dr. James Middleton for starting the ice-phobic research and guidance. I must also thank Monika Bleszynski for her valuable insight and assistance in the experimental work. I also appreciate the work done by Dan Waters, who help set up and build the ice adhesion test apparatus. Finally, I express my gratitude to my family for their unwavering support.

Table of Contents

Chapter One: Introduction	1
General introduction	1
Literature Review.....	3
Chapter Two: Finite element Analysis of the Ice Block Adhesion Test.....	18
Introduction.....	18
Methods.....	18
Results.....	24
Discussion.....	41
Chapter Three: Experimental Evaluation of Mold Type and Substrate Thickness on Ice Adhesion	44
Introduction.....	44
Methods.....	44
Results.....	49
Discussion.....	55
Chapter Four: Effects of Crosslink Density and Aging of PDMS Substrates on Ice Adhesion	58
Introduction.....	58
Methods.....	58
Results.....	59
Discussion.....	64
Chapter Five: Summary and Conclusion	66
Summary.....	66
Conclusion	67
Works Cited	69
Appendix - Acronyms and Symbols	73

List of Figures

Chapter One	1
Figure 1	4
Figure 2	5
Figure 3	6
Figure 4	8
Figure 5	9
Figure 6	10
Figure 7	12
Figure 8	13
Figure 9	15
Chapter Two.....	18
Figure 10	21
Figure 11	21
Figure 12	23
Figure 13	25
Figure 14	26
Figure 15	28
Figure 16	31
Figure 17	33
Figure 18	36
Figure 19	37
Figure 20	38
Figure 21	39
Chapter Three	44
Figure 22	47
Figure 23	48
Figure 24	49
Figure 25	51
Figure 26	52
Figure 27	54
Chapter Four	58
Figure 28	62
Figure 29	63

List of Tables

Chapter One	1
Table 1	17
Chapter Two	18
Table 2	22
Table 3	22
Table 4	26
Table 5	28
Table 6	32
Table 7	40
Table 8	40
Chapter Three	44
Table 9	54
Chapter Four	58
Table 10	60
Table 11	61
Table 12	62

Chapter One: Introduction

General introduction

Ice and frost accumulation is a major concern for many different industries. For example, ice, snow, and wetness accounts for 40% of the reported car accidents during winter [1]. Ice accumulation can also cause the downing of power lines and ground both airplanes and helicopters [2]. Furthermore, the accumulation of ice on wind turbine blades can lead to 50% loss in annual power production [1]. Current methods for removing ice involve using mechanical, thermal, or chemical approaches [1, 3]. Mechanical methods typically involve removing ice buildup by scrubbing or scrapping it off, such as in freezers or heat exchangers. Thermal methods involve heating the surface in contact with the ice to melt the ice off the surface. Chemical methods involve spraying the surface with organic liquids to lower the freezing point of the ice and thus preventing the ice from forming.

The problem with the above methods are that they are slow, costly, and require frequent repeated application. This has led to research into alternative methods for ice prevention and removal; such as ice releasing, or ice-phobic, materials. Ice-phobic materials are materials that can resist ice buildup and adhesion. Typically, a material requires a weak adhesion strength to ice, less than 100 kPa to shear the ice from the surface, to be categorized as an ice-phobic material [4]. Ice-phobic materials present a passive

method for removing ice by allowing ice to be dislodged through vibrations, strong winds, centrifugal forces, or due to the weight of the ice.

The ideal ice adhesion test involves generating only shear stress at the interface between the ice and ice-phobic material. Dynamic factors such as torque need to be eliminated or minimized to get close to the ideal ice adhesion test. Torque adds rotation and normal stresses to the system; which means that the test would no longer be measuring only the shear strength. The test would instead be a mix mode failure caused by both shear and peeling. Also, an ideal ice adhesion test should only have cohesive or adhesive failures. Adhesive failures are failures that occur at the interface between the substrate and the adhesive; whereas, cohesive failures are failures that occur inside the bulk of the adhesive material [5]. The failure for an ice-phobic material should be strictly an adhesive failure in which no ice remains on the surface.

Literature Review

Some early research into ice releasing involved examining ice adhesion on super-hydrophobic surfaces (SHSs). Water beads up on SHSs and has extremely high contact angles ($>150^\circ$). These surfaces also have small contact angle hysteresis, which means that water rolls off the surfaces at relatively low angles. The benefit to SHSs is that water can shed before it has a chance to freeze [1, 6-8]. However, water that freezes on the SHS has a minimized contact area due to its geometry. SHSs have micro- and nano-pillars on the surface in which trapped air sits. When the SHSs are in a non-wetted, or Cassie-Baxter state, the water sits on top of the pillars minimizing the contact to the surface. Thus, the ice has less area to adhere to the surface. However, there is an increase in ice adhesion strength if the SHSs enters the Wenzel or wetted state, as shown in Figure 1. Water sitting on the surface can penetrate the area around the micro- and nano- pillars over time and force out the air between the pillars, causing the surface to become wetted. There is also a possibility for small enough water droplets, i.e. fog, to be able to enter the area around the pillars with ease or for rain droplet hitting the surface fast enough to instantly enter the Wenzel state. The ice formed in the Wenzel state has more area to adhere to and interlocks between the pillars. Thus, causing greater ice adhesion to the SHS. The removal of ice can also damage the pillars and over time deteriorate the surface, which causes it to lose its water shedding ability and ice-releasing properties.

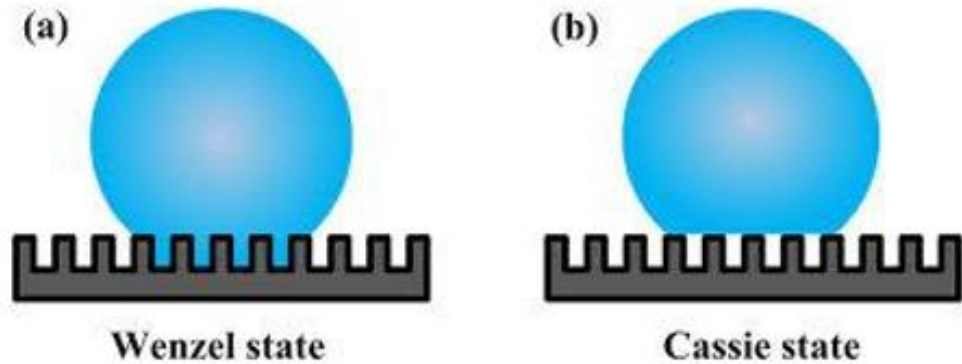


Figure 1: Water droplet in the Wenzel state (a) and the Cassie state (b). Water frozen in the Wenzel state has higher ice adhesion strength due to the interlocking between the ice and pillars. Also, removal of ice in this state can damage the pillars. This Figure was copied from [9].

Another approach, similar to the SHSs, is to design a surface in which liquid, instead of air, is trapped between the pillars. These surfaces are called slippery liquid-infused porous surfaces (SLIPS) and typically involve infusing a low energy surface, such as Teflon, with a pre-fluorinated fluid [1]. The fluid forms a continuous lubricating layer on the surface and creates a slip boundary between the ice and the surface. This lubricating layer allows for easy removal of ice and provides extremely low ice adhesion, as depicted in Figure 2. However, the ice removes some of the liquid each time the ice is dislodged from the surface [1, 4]. Thus, over time the fluid is depleted from the surface and the anti-icing properties of the surface are lost.

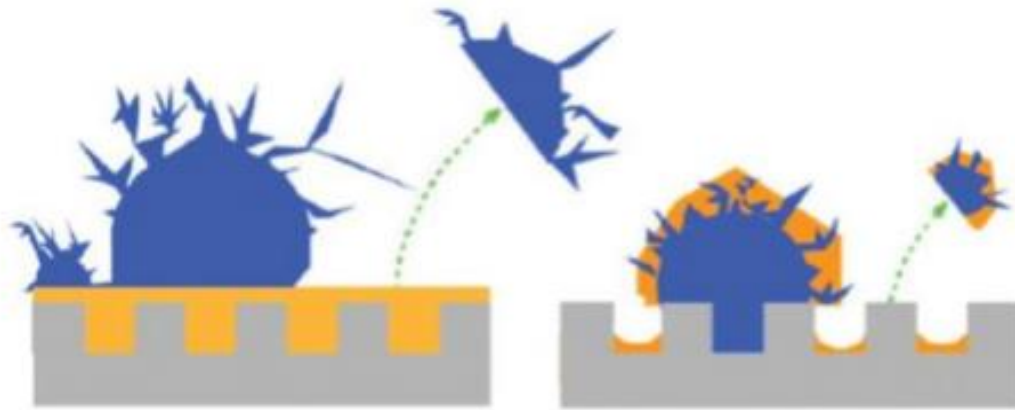


Figure 2: Depiction of ice being shed from the lubricating boundary. The slip boundary allows for low ice adhesion, less than 20kPa, but the lubricated layer is reduced each time ice is shed. This Figure was copied from [1].

Materials with natural low ice adhesion, such as elastomers, are also receiving attention [3,4]. Studying these materials has led some researchers to propose that ice adhesion strength on soft materials is expressed by equation 1 below [3]. The equation suggests that the ice adhesion strength (τ) is affected by the surface's shear modulus (μ), the thickness of the sample (t), and the work of adhesion between the ice and surface (W_{adh}). The equation was developed for thin film samples and does not apply to bulk materials because the thickness ceases to affect ice adhesion after the material reaches a certain size. The shear modulus can easily be manipulated by controlling the crosslinking density of the elastomers [3,4]. The shear modulus decreases as the crosslinking density decreases and thus the ice adhesion should decrease with reduced crosslinking. Figure 3 shows the results from a group at Colorado State University that formulated a Polydimethylsiloxane, PDMS, silicon rubber coating [3]. The group mixed together vinyl-terminated PDMS, hydride-terminated PDMS, and trimethyl-terminated PDMS, t-PDMS.

The t-PDMS was nonreactive and would limit the amount of crosslinking formed in solution, thus controlling the amount of crosslinking in their samples. Their results showed that both the shear modulus and ice adhesion strength decreased as the amount of unreacted PDMS increased. However, the researchers found that if the crosslinking density was too low then the PDMS would either form a gel or not solidify.

$$\tau \sim \sqrt{\frac{W_{adh}\mu}{t}} \quad (1)$$

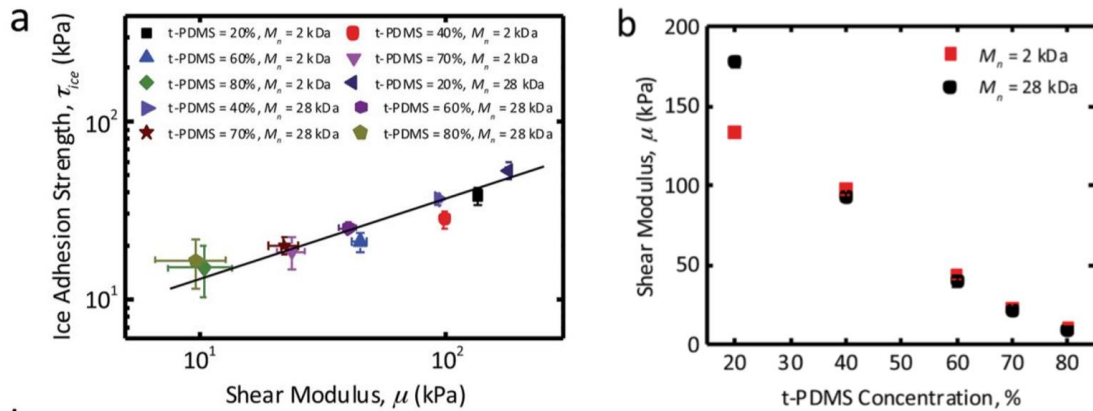


Figure 3: Ice adhesion strength as a function of shear modulus (a) and shear modulus as a function of t-PDMS concentration (b). The shear modulus decreased as t-PDMS concentrations increased. Also, lower shear moduli resulted in lower ice adhesion strengths. Thus, showing that elastomers with lower crosslink densities produce low ice adhesion strengths. These Figures were copied from [3].

For PDMS, there are three main types of curing processes: peroxide curing, addition curing, and condensation curing. Peroxide curing, typically found in high

temperature vulcanized rubbers, does not require a catalyst for the reaction to occur [10]. However, free radicals need to be generated for peroxide curing to take place, as shown in Figure 4. Thus, peroxide cures need to be heated or irradiated for the reaction to occur. In contrast, addition and condensation curing does not need to be irradiated and can occur at room temperature, though addition curing will cure in less time if heated. Addition and condensation curing do require a catalyst for the reaction to occur, as shown in Figure 5 and Figure 6. Addition curing typically uses platinum as a catalyst; whereas, condensation curing typically uses tin. The properties of addition cured, and condensation cured PDMS are usually slightly different [11]. For example, addition cures typically are heat resistant and are more suitable for higher temperature environments than condensation cures. In addition, platinum-catalyzed PDMS is typically more resistant to tearing than tin-catalyzed PDMS. However, condensed cured PDMS is cheaper to produce than addition cures and requires a lower amount of catalyst.

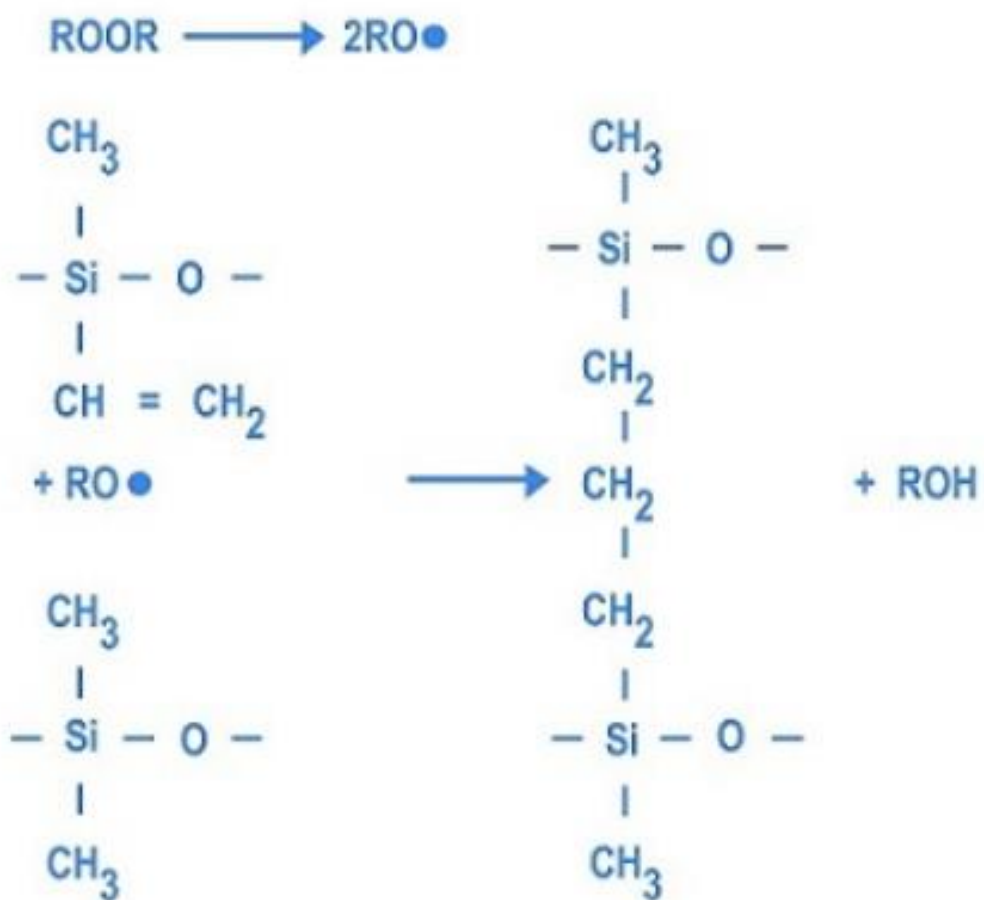


Figure 4: Reactions for peroxide curing of PDMS. This Figure was copied from [10].

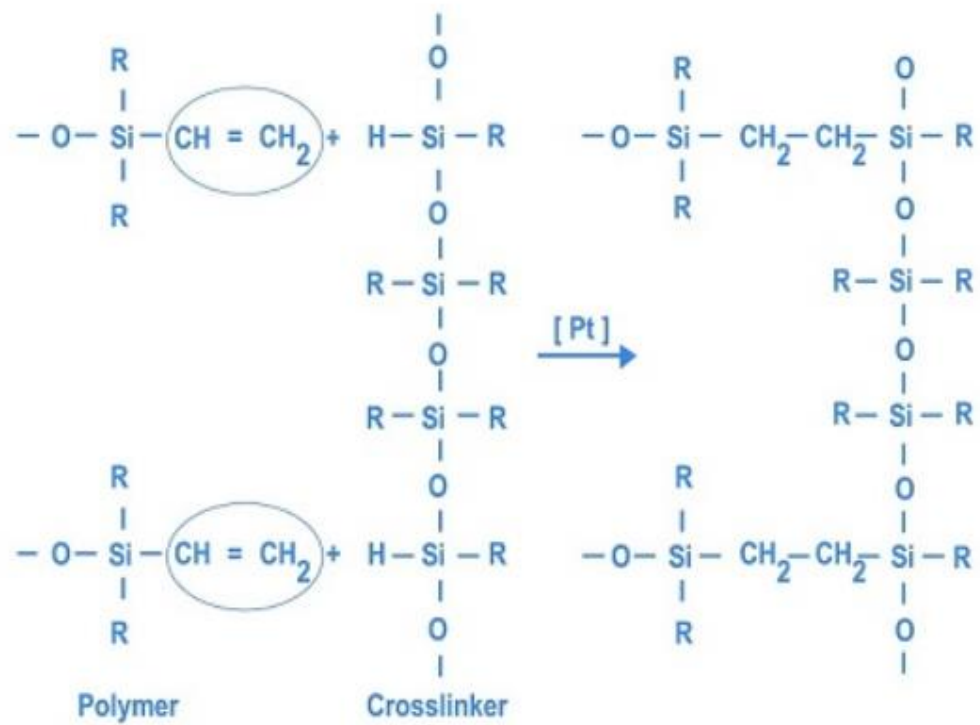


Figure 5: Reactions for addition, platinum catalyzed, curing of PDMS. This Figure was copied from [10].

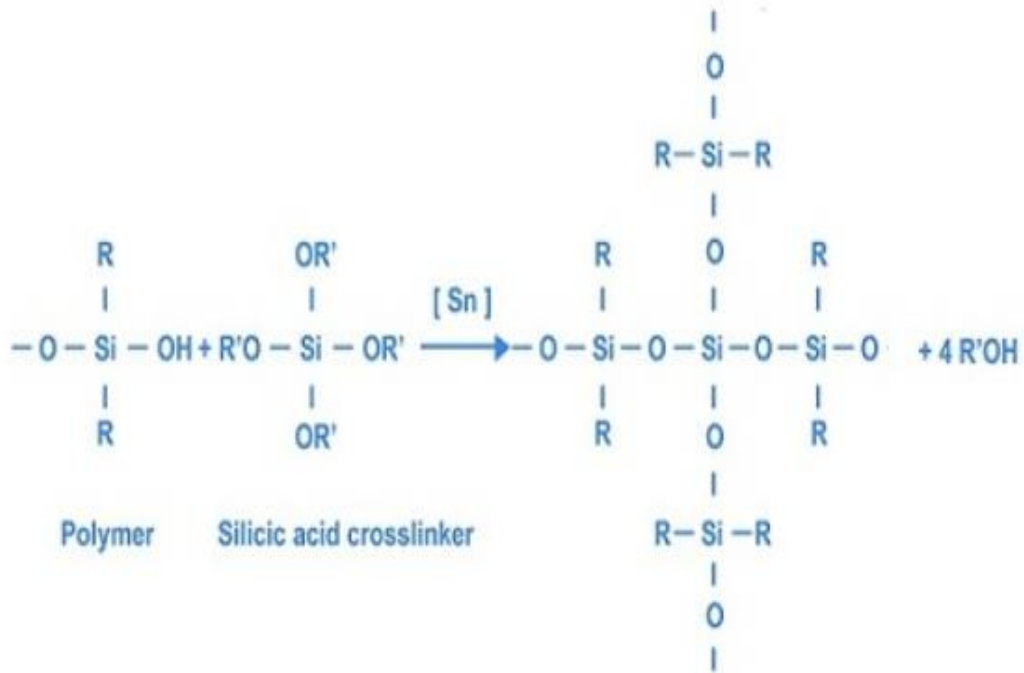


Figure 6: Reactions for condensation, tin catalyzed, curing of PDMS. This figure was copied from [10].

Ice Adhesion Testing

Currently, there is no standard for testing ice adhesion strength and, testing is neither straightforward nor consistent. As a result, research groups have developed various methods for testing ice adhesion. For example, Ozbay et al. developed a method in which 50 μL water droplets are placed on a surface at room temperature and then moved to a $-30\text{ }^\circ\text{C}$ chest freezer [12]. The surface is left in the freezer for 15 minutes before it is moved to a climatic chamber with a relative humidity of $58\% \pm 3\%$ RH at $-10\text{ }^\circ\text{C}$. The surface is again left alone for 15 minutes before a probe, located 1 mm above the surface, is pushed against the frozen water droplet at a constant velocity of 0.025mm/s using a 2D plunger. The forces (F) needed to dislodge the frozen water droplet are recorded using a force transducer and then divided by the contact area (A) to determine the ice adhesion strength (τ), as shown in equation 2. Equation 2 is used in most ice adhesion tests to determine the ice adhesion strength.

$$\tau = \frac{F}{A} \quad (2)$$

Another test used by Bharathidasan et al. involved using a custom-built instrument, shown in Figure 7, based on the zero-degree cone test developed by Haehnel and Mulherin [13-15]. The system consists of an inner cylindrical aluminum pin and an outer cylindrical mold. The pin is centered in the mold by using a Teflon bush located at the bottom of the

system. The pins are polished and coated with test samples beforehand. The gap between the pin and the mold is then filled with deionized water and the water is frozen by keeping the assembly in a chest freezer, maintained at $-20\text{ }^{\circ}\text{C}$ for 24 hours. Bharathidasan et al. modified the zero-degree cone test by adding a cooling jacket containing brine solution. The cooling jacket is used to maintain the temperature during the test and the temperature of the system can be adjusted by varying the brine concentration. The pin is then either pulled out of the ice or rotated using a servo motor until the bonds between the ice and sample are broken. The maximum force needed separate the sample from the ice is recorded using a load cell. The adhesion strength is then calculated by dividing the maximum force by the contact area.

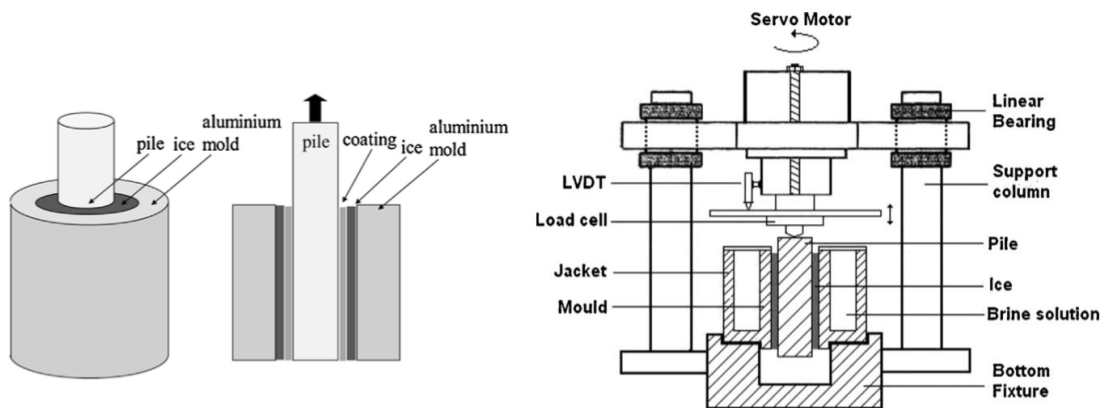


Figure 7: Zero-degree cone test with brine solution cooling jacket. These figures were copied from [13, 14].

A third method used by Jafari et al. involves a custom-made centrifuge, shown in Figure 8. This test involves attaching the test sample to one end of an aluminum beam and then placing the beam in a refrigerated wind tunnel [16-20]. Water droplets, $\sim 80\text{ }\mu\text{m}$ diameter, are feed into the wind tunnel and wind speeds of 10 m/s deposit the droplets on

the sample. The tunnel's temperature is kept at $-10\text{ }^{\circ}\text{C}$ and an ice layer, approximately 1 cm thick, is formed on the sample. The beam is then attached to a centrifuge at $-10\text{ }^{\circ}\text{C}$ and a counter weight is attached to the beam on the opposite side of the sample. The centrifuge then begins to spin at increasing speeds until the ice is dislodged. The force needed to dislodge the ice layer is then calculated using equation 3, where m is the mass of ice, r is the beam radius, and ω is the rotation speed.

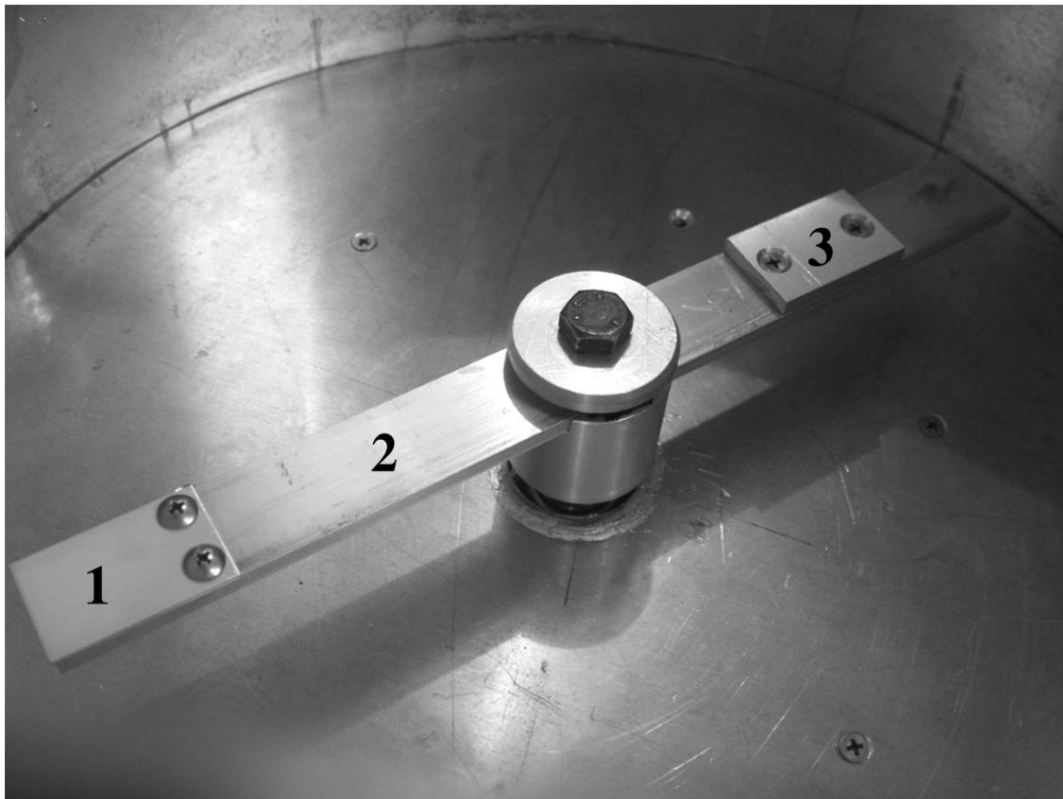


Figure 8: Centrifuge used by Jafari et al. to test ice adhesion, (1) the sample on which ice is deposited, (2) aluminum beam, (3) counter weight. This Figure was copied from [18].

$$F = mr\omega^2 \quad (3)$$

A fourth method has also been used by Ling et al and Fu et al., which involves forming an ice cube on top of the sample using a mold [21, 22]. Ling et al apparatus, shown in Figure 9, clamped the samples to an air-cooled thermoelectric Peltier cooling unit, or cold plate. The cold plate temperature is dropped to $-15\text{ }^{\circ}\text{C}$ and a borosilicate glass tube is placed on top of the sample. Approximately 0.5 mL of reverse osmosis, RO, water is pipetted into the glass tube and left to freeze. Another 1.5 mL of water is then pipetted into the glass tube and given 2 hrs to freeze. A linear stage, moving with a velocity of 0.5mm/s, was used to push a piston against the glass tube and a force gauge was used to record the force needed to dislodge the ice. Equation 2 was then used to calculate the ice adhesion strength. Fu et al. had a similar setup; however, the experiment took place in a weather chamber and compressed air was used to push the force gauge into a 18mm by 18mm Teflon mold with a sealed bottom. The weather chamber temperature was set to $-10\text{ }^{\circ}\text{C}$ before the test and the Teflon mold was filled with DI water. The sample was then placed on top of the Teflon mold, flipped over, and given 3 hours to freeze. An air cylinder was then used to push the force gauge into the ice block at a rate of 12.5 N/s until the ice is dislodged. The adhesion strength was then calculated using equation 2.

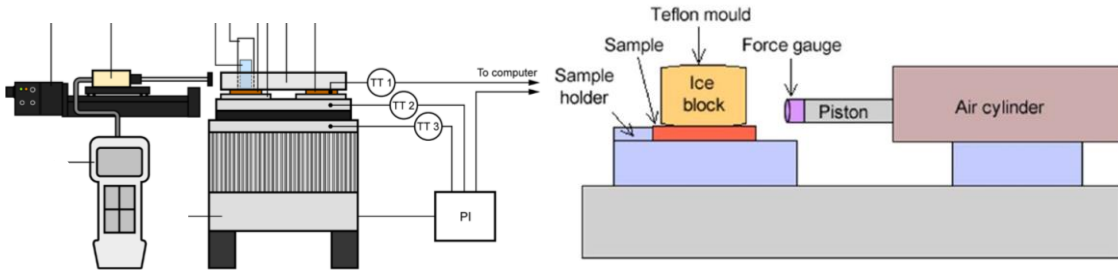


Figure 9: Ling et al. (left) and Fu et al. (right) schematics for the ice adhesion block test. These Figures were copied from [21,22].

Another variation to the ice cube test used by Kim et al.; used custom made hydrophobic cylindrical glass columns [23]. Well polished Pasteur pipettes, with a 24 mm inner diameter, were cut to make the columns. The columns were made hydrophobic by treating them with oxygen plasma for 60 seconds and then leaving them in a vacuum with (tridecafluoro-1, 1, 2, 2-tetrahydrooctyl) for 24 hours. Samples were attached to a cold plate using thermally conductive tape. Then, the columns were placed on top of the samples and filled with 150 μ l of water. The set-up took place inside an environmental chamber to control humidity during the experiments. The humidity was below 3% RH at the beginning of the experiment and then the chamber was cooled at a rate of 2 $^{\circ}$ C/min until the temperature reached -20 $^{\circ}$ C. The chamber's temperature was brought up to -10 $^{\circ}$ C after ice formation was observed and the system was given 30 minutes to equilibrate. The adhesion strength was then tested using a custom force gauge that could either push or pull on the column.

Table 1 shows the measured ice adhesion strength for various materials using the tests mentioned above. The most direct test methods were the centrifuge test and the ice

cube test, which has the added benefit of easy setup. A test setup similar to Ling et al [21] was chosen to evaluate the ice adhesion strength of PDMS, expressed in chapters 3 and 4.

Table 1: An overview of typical materials and their corresponding ice adhesion strengths.

Material	Average Ice Adhesion Strength [kPa]	Report
Copper - 50 μ L water droplets placed on the test surface by a syringe	1217 \pm 34	Ozbay et al. [12]
Polished Copper - 2.4 \pm 0.15 mm thick borosilicate glass tube mold	625 \pm 41	Ling et al. [21]
Stainless steel 316 - 2.4 \pm 0.15 mm thick borosilicate glass tube mold	682 \pm 46	Ling et al. [21]
Aluminum - 50 μ L water droplets placed on the test surface by a syringe	731 \pm 53	Ozbay et al. [12]
Polished aluminum - centrifuge adhesion	250 \pm 50	Jafari et al. [19]
Glass – upside-down Teflon mold	820 \pm 96	Fu et al. [22]
PTFE - 50 μ L water droplets placed on the test surface by a syringe	268 \pm 13	Ozbay et al. [12]
RF-sputtered PTFE coating on polished aluminum - centrifuge adhesion test	110 \pm 22	Jafari et al. [19]
RF-sputtered PTFE coating on anodized surface - centrifuge adhesion test method	72 \pm 12	Jafari et al. [19]
RTV silicone rubber coating – customized zero-degree cone test method	24.8 \pm 8	Bharathidasan et al. [13]
RTV coating with fumed silica particles - customized zero-degree cone test method	243 \pm 20	Bharathidasan et al. [13]
Slippery, liquid-infused porous surfaces (SLIPS) - Cylindrical glass column mold made from Pasteur pipette	15.6 \pm 3.6	Kim et al. [23]
Dragon skin 20 (RTV silicone rubber) - PDMS removable mold	34.63 \pm 4.20	University of Denver

Chapter Two: Finite element Analysis of the Ice Block Adhesion Test

Introduction

Finite element methods (FEM) were used to better understand the ice adhesion test, originally proposed by Ling, et al [21], and its limitations. The FEM models examined different scenarios such as the mold effect, piston height, substrate thickness, and others, and their effects on the ice adhesion results.

Methods

The FEM Modelling was done using the COMSOL Multiphysics basic package. The FEM models were 2D linear elastic and were 25.4 mm thick (the thickness going into the page). The ice was modelled as being encased in either a polycarbonate mold, a steel mold, or free of a mold. The dimensions of the ice block, free of the mold, were 25.4 mm by 25.4 mm. The dimensions of the ice, encased in the mold, were 22.22 mm wide by 25.4 mm high. The dimensions of the polycarbonate and steel molds were 15.87 mm wide by 25.4 mm high. The substrate surface was initially modelled as PDMS with dimensions of 1000 mm in length by 3mm in height. The bottom of the PDMS was fixed and the ice/mold/substrate interfaces were assumed to form a perfect union, thus they could not be separated. A rectangular piston was modeled as applying pressure to the left wall of either

the mold or ice. The piston dimensions were 13 mm high and 2 mm wide. The piston was initially set 3 mm above the PDMS surface. A pressure of 19.53 kN/m² was applied to the mold or ice, which corresponded to a total force of 1.45 lb_f.

Figure 10 shows a basic schematic of the ice block model. The mesh for the ice block consisted of 2664 triangular elements with a mesh area of 9.84E⁻⁴ m. The average element quality was 0.9814 and the minimum mesh quality was 0.762. The mesh for encapsulated ice consisted of 2750 triangular elements with a mesh area of 9.712E⁻⁴ m. The average element quality was 0.9712 and the minimum mesh quality was 0.791. Thus, the average mesh quality in these models was acceptable. Table 2 shows the mesh statistics given by COMSOL and Figure 11 depicts the encapsulated and ice block models after the mesh was created. Table 3 shows the material properties for the PDMS, steel, polycarbonate, which came from a built-in library in COMSOL [24], the PC properties came from Professional Plastics data sheet [25], and the ice properties came from [26].

Initially, a simulation using the ice block model was used to gain an idea of how the system might deform during the test. The steel encapsulated ice model was then used as a comparison. A wedge was placed between the steel mold and the PDMS substrate. This was done to understand how a gap between the mold and substrate would affect the ice adhesion results. Figure 12 depicts the FEM model when wedges are added to the mold on both sides of the mold. Initially, the wedge had an angle of 0.1° and a width of 15.87 mm, the same width as the steel walls. The wedge was first filled with ice, then the ice was removed; leaving an empty gap. The angle of wedge was then changed to 1°, 2°, 3°, and 4° to increase the size of the empty gap.

The piston position was adjusted to explore its effect on the ice displacements. The ice block model was used for these simulations. The piston was placed 0.1 mm above the PDMS surface, with the distance measured from the bottom of the piston to the PDMS surface. The height was then gradually increased until the piston was 25.3 mm above the surface. The next simulation involved changing the PDMS thickness to evaluate how it affects deformation, in the substrate, and displacements, at the ice-PDMS interface. The piston's position was moved back to 3 mm above the PDMS surface and the ice block model was used. The thickness of the PDMS was changed to 0.1 mm and was then gradually increased to 50 mm.

The final set of simulations involved changing the stiffness of the substrate. The ice block model was used for these simulations. The substrate was initially modelled using the properties of PDMS but was then changed to have the properties of polycarbonate followed by steel. The substrate had a thickness of 3 mm. The substrate properties were then changed back to PDMS but, the Young's modulus was gradually increased from 750 kPa to 50 GPa. For the last model, the substrate thickness was first set to 3mm but was then changed to 8mm.

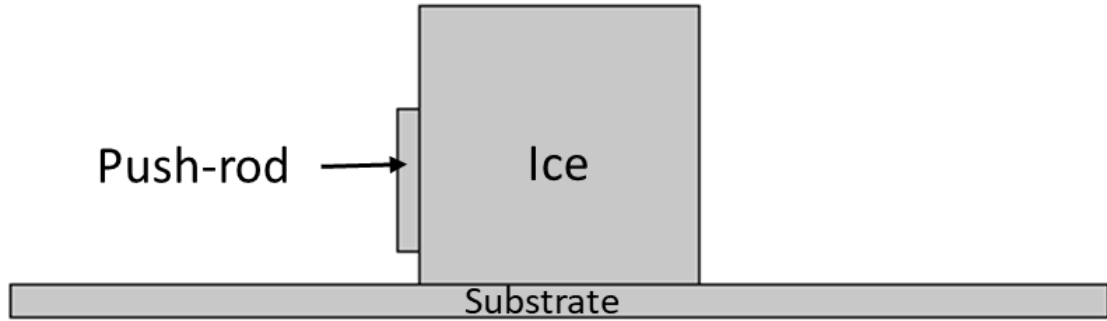


Figure 10: Schematic of the ice block model with a piston for the test without a mold.

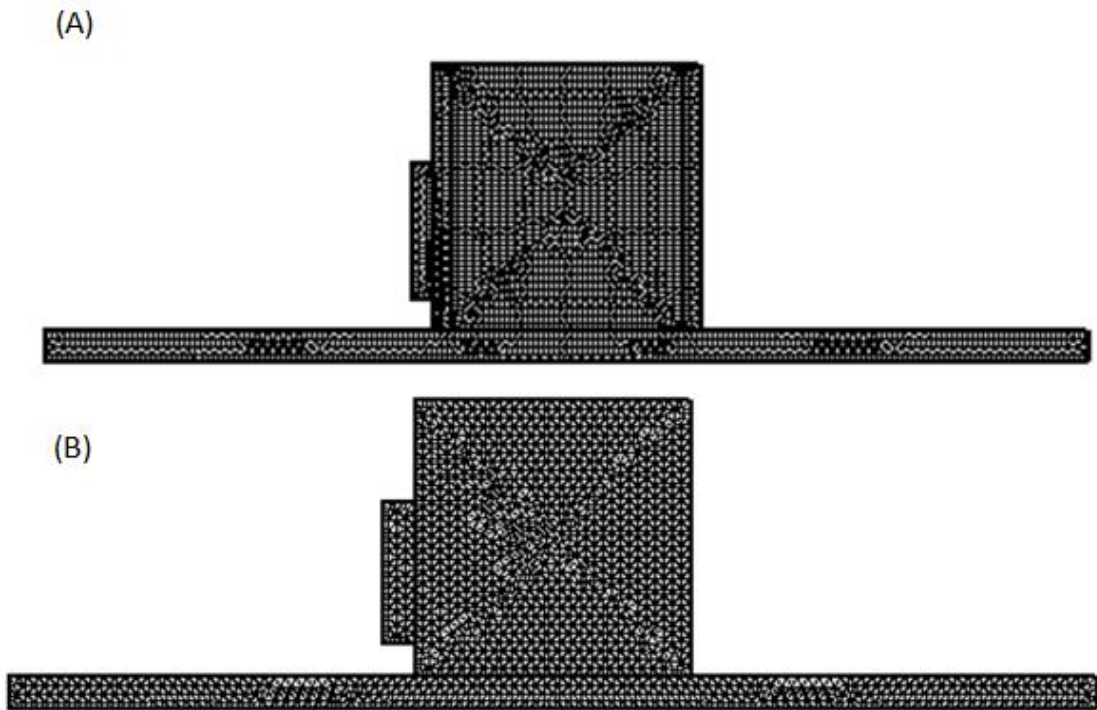


Figure 11 (A, B): Finite element meshes used to analyze the ice block displacements and stresses with (A) and without (B) a mold.

Table 2: Properties of meshes used in the numerical analysis.

Mesh Details	Ice with Walls	Ice without Walls
Triangular Elements	2750	2664
Edge Elements	367	305
Vertex Elements	16	12
Number of Elements	2750	2664
Average Element Quality	0.97778	0.9814
Minimum Element Quality	0.791	0.762
Mesh Area Ratio	$9.712E^{-04}$	$9.84E^{-04}$

Table 3: Material properties used for the FE models.

Material	Density (kg/m ³)	Poisson's Ratio	Young's Modulus (GPa)
PDMS	970	0.49	$7.50E^{-4}$
Steel AISI 4340	7850	0.28	205
Polycarbonate	1220	0.37	2.40
Ice	916.7	0.31	9.00

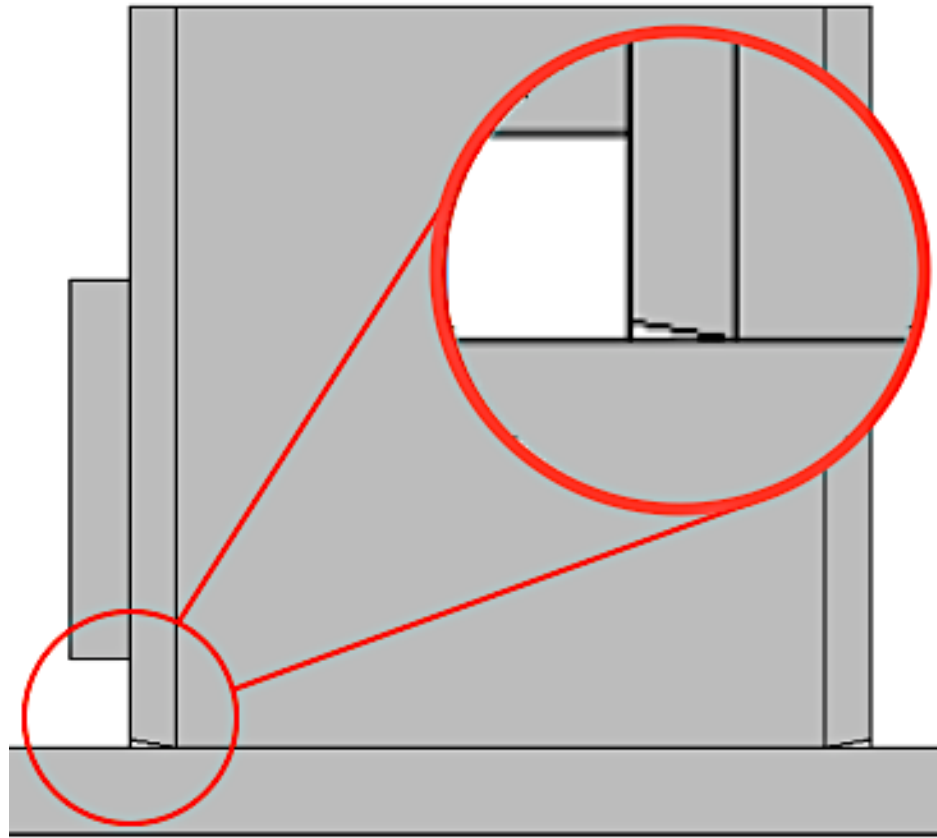


Figure 12: Schematic of a model with a separation between the mold and the substrate.

Results

Figure 13 depicts an exaggerated model showing the deformation of the ice block and the PDMS substrate. The model shows that the side of the ice being pushed on will lift and the opposite side will embed into the substrate. The max vertical displacement on the lifted side was $8.74 \mu\text{m}$ and the embedded side had a max vertical displacement of $-8.74 \mu\text{m}$. Thus, the ice block edges experienced equal and opposite displacements. Figure 14 shows

the max vertical displacements for the encapsulated ice model after the wedges were assumed. The wedge models showed the same trend in which the side being pushed upon was lifted and the opposite was embedded into the substrate. The max vertical displacement was $8.78\ \mu\text{m}$ for the situation in which the wedge was filled with ice. Thus, the ice block model and wedge model produced similar displacements. However, the vertical displacement increased by 77.98% after the ice wedge was removed, leaving a gap between the steel mold and PDMS substrate. Furthermore, the vertical displacement decreased from $15.63\ \mu\text{m}$ to $13.74\ \mu\text{m}$ as the wedge angle increased from 0.1° to 1° . This corresponded to a 12.07% drop in the vertical displacement. The vertical displacement for the 1° empty wedge model was still 56.49% higher than the ice wedge model, increasing the gap angle further from 1° to 2° , 3° , or 4° had a negligible impact on the vertical displacement.

The horizontal displacement also increased slightly when the wedge without ice was modeled. The horizontal displacement increased by 9.73% after the ice was removed from the gap and varied only by 0.7% as the gap increased from 0.1° to 4° . This caused the ratio of vertical to horizontal displacements to increase from 0.10:1 to 0.16:1 when the ice wedge was replaced with an empty gap, which corresponded to a 62.5% increase in the ratio of vertical to horizontal displacements. However, the ratio of the vertical to horizontal displacements dropped to 0.137:1 as the gap angle increased to 4° ; which resulted in the ratio of the vertical to horizontal displacements only being 42.71% higher than in the ice wedge model. Table 4 summarizes the max vertical and horizontal displacements caused by adding and enlarging the wedge.

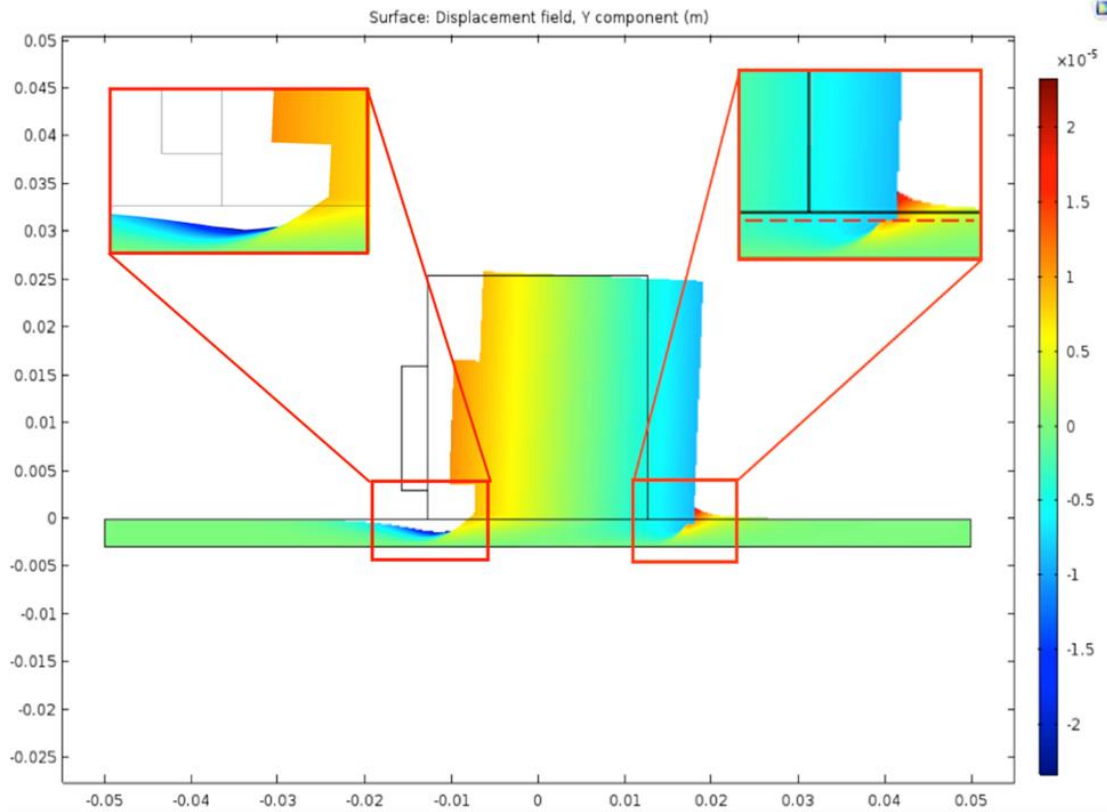


Figure 13: An exaggerated model of a deformed ice cube, without a mold encasement, after shearing, and the ice cube's bottom right corner (in red) where the red dotted line represents where the edge of the cube is after shearing. The solid black lines represent the model before shearing.

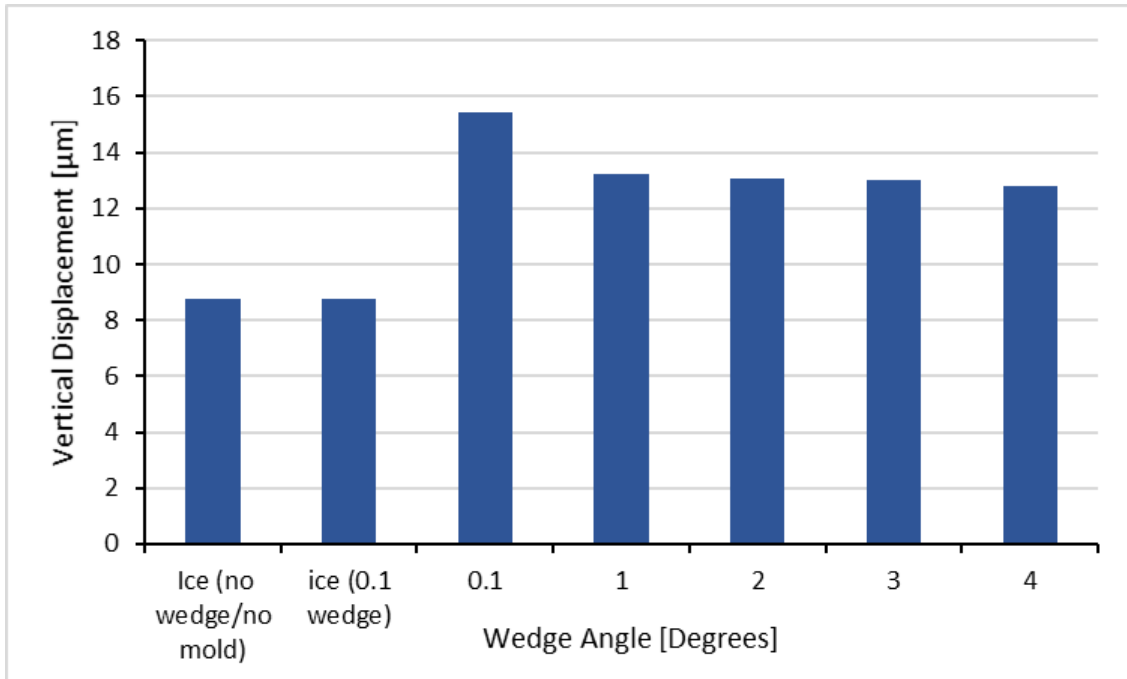


Figure 14: Vertical displacement as a function of a wedge crack angle. These values were from the FEM analysis.

Table 4: The effect of wedges on max displacements and the ratios of the horizontal to vertical displacements. These values were from the FEM analysis.

Wedge angle (degrees)	Vertical displacements (µm)	Horizontal displacements (µm)	Horizontal: Vertical Displacement	Vertical: Horizontal Displacement	Change in Vertical Displacement (%)	Change in Horizontal Displacement (%)
ice (0.1 wedge)	8.78	91.71	10.45:1	0.10:1		
0.1	15.63	100.4	6.43:1	0.16:1	77.98	0.19
1	13.74	100.18	7.29:1	0.14:1	56.49	0.04
2	13.68	99.97	7.31:1	0.14:1	55.80	0.24
3	13.59	99.88	7.35:1	0.14:1	54.78	0.21
4	13.67	100.05	7.32:1	0.14:1	55.69	0.22

Figure 15 shows the max vertical displacement as a function of push rod position. The max vertical displacement was $4.27\ \mu\text{m}$ when the piston was $0.1\ \text{mm}$ above the substrate. The vertical displacements then increased to $8.74\ \mu\text{m}$ after being moved to $3\ \text{mm}$ above the substrate; which resulted in the vertical displacement being approximately 105% higher than when the piston was $0.1\ \text{mm}$ above the substrate. The highest placement of the piston was $25.3\ \text{mm}$ above the substrate, at which point only the bottom of the piston was in contact with the ice. The max vertical displacement was $42.71\ \mu\text{m}$ when the piston was in this location; which corresponded with the displacement being approximately 10 times higher than when the piston was $0.1\ \text{mm}$ above the substrate. It should also be noted that the max vertical displacements increased linearly as the piston was moved to higher positions.

The displacements in the horizontal direction also increased slightly as the piston moved upwards. However, the change in the horizontal displacements was less than 1% as the piston moved from $0.1\ \text{mm}$ to $25.3\ \text{mm}$ above the substrate. Thus, the ratio between the horizontal and vertical displacements decreased as the push rod was lifted. This corresponded with the ratio between the vertical and horizontal displacements increasing from 0.05:1 to 0.45:1, approximately a 9-fold increase, as the piston moved from $0.1\ \text{mm}$ to $25.3\ \text{mm}$ above the surface. Table 5 shows the max horizontal and vertical displacements, and the ratios between them as a function of piston position.

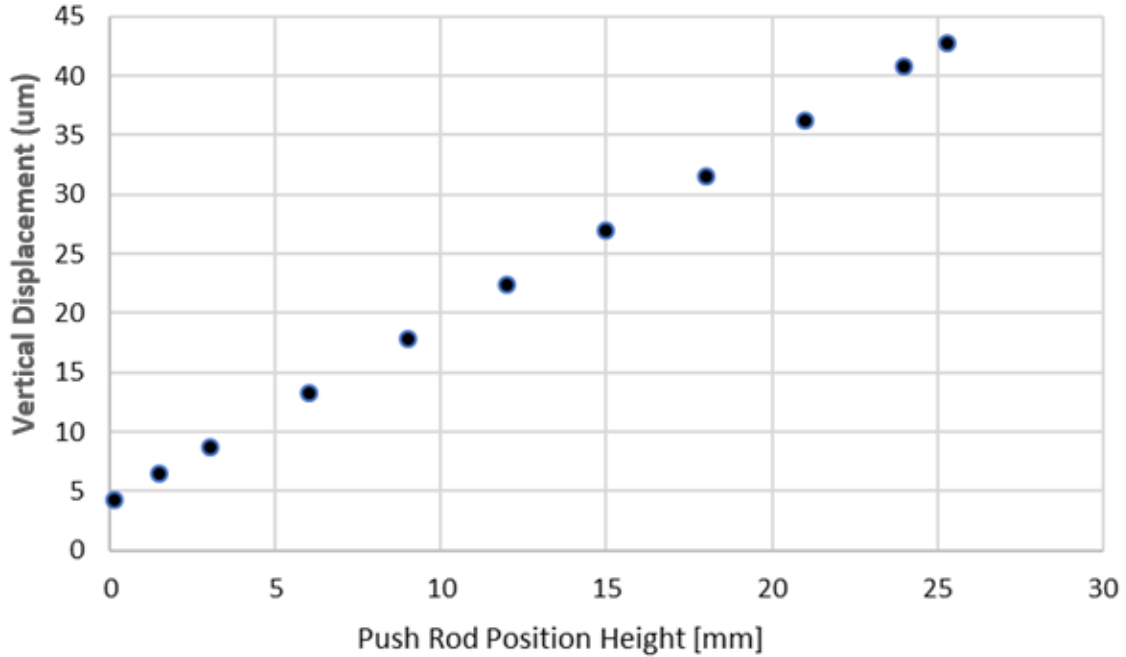


Figure 15: Max vertical displacement as a function of push rod position. These values were from the FEM analysis.

Table 5: Effect of push rod position on max displacements and ratios of horizontal to vertical displacement. These values were from the FEM analysis.

Piston Distance from Surface (mm)	Vertical Displacements (µm)	Horizontal Displacements (µm)	Horizontal: Vertical Displacement	Vertical: Horizontal Displacement
0.1	4.27	93.79	21.96:1	0.05:1
1.5	6.48	93.52	14.44:1	0.07:1
3	8.74	93.52	10.70:1	0.09:1
6	13.31	93.57	7.03:1	0.14:1
9	17.88	93.62	5.24:1	0.19:1
12	22.45	93.67	4.17:1	0.24:1
15	27.02	93.72	3.47:1	0.29:1
18	31.59	93.78	2.97:1	0.34:1
21	36.16	93.83	2.60:1	0.39:1
24	40.73	93.88	2.31:1	0.43:1
25.3	42.71	93.91	2.20:1	0.45:1

Figure 16 shows the max vertical displacement at the ice/substrate interface as a function of sample thickness. The max vertical displacement was $0.26\ \mu\text{m}$ when the sample was $0.14\ \text{mm}$ thick. The max vertical displacement increased to $1.89\ \mu\text{m}$ when the substrate was $1\ \text{mm}$ thick and then increased to $8.74\ \mu\text{m}$ for the $3\ \text{mm}$ substrate. Furthermore, increasing the thickness to $50\ \text{mm}$ resulted in a $237.22\ \mu\text{m}$ vertical displacement. This corresponded with the vertical displacement increasing by approximately 7-fold as the substrate thickness increased from $0.14\ \text{mm}$ to $1\ \text{mm}$ and an 840-fold increase as the thickness of the substrate went from 0.14 to $50\ \text{mm}$. Thus, it can be seen in Figure 16 that the vertical displacement at the ice-PDMS interface increased as the substrate thickness increased. It should also be noted that the change in the vertical displacement becomes less drastic after the substrate became thicker than $25\ \text{mm}$.

The displacement in the horizontal direction also increased as the PDMS substrate thickness increased. The max horizontal displacement was $5.57\ \mu\text{m}$ when the substrate was $0.14\ \text{mm}$ thick and then increased to $36.46\ \mu\text{m}$ when the substrate thickness was increased to $1\ \text{mm}$. This was followed by the horizontal displacement increasing to $838.57\ \mu\text{m}$ at $50\ \text{mm}$ thick. This corresponded to the horizontal displacement increasing by approximately 7-fold as the substrate thickness increased from $0.14\ \text{mm}$ to $1\ \text{mm}$ and approximately 150-fold as the substrate went from 0.14 to $50\ \text{mm}$ thick. Thus, the changes in the horizontal displacement were not as drastic as the changes in vertical displacement. This lead to the ratios between the vertical displacement and horizontal displacement to increase as the thickness increased. Table 6 presents the max horizontal displacements, the max vertical displacements, and the ratios between them as a function of substrate thickness. The table

also show that the ratios between the vertical and horizontal displacements increased from 0.05:1 to 0.28:1 as the thickness increased from 1mm to 50mm.

The interfacial normal stresses at the ice-PDMS interface were also examined for the substrate thickness ranging from 0.14 mm to 1.1 mm. Figure 17 shows the normal stresses at the ice-PDMS interface. The figure also presents that changing the thickness did not cause much variation in the normal stresses at the interface, except at the edges. The normal stresses at the edges were highest for the 1.1 mm thick substrate and minimum for the 0.14 mm thick substrate. It should also be noted that the normal stresses are in tension on the edge where the force was applied, i.e. the edge was lifted. On the compressive side, on the opposite edge, i.e. the edge was imbedded into the PDMS.

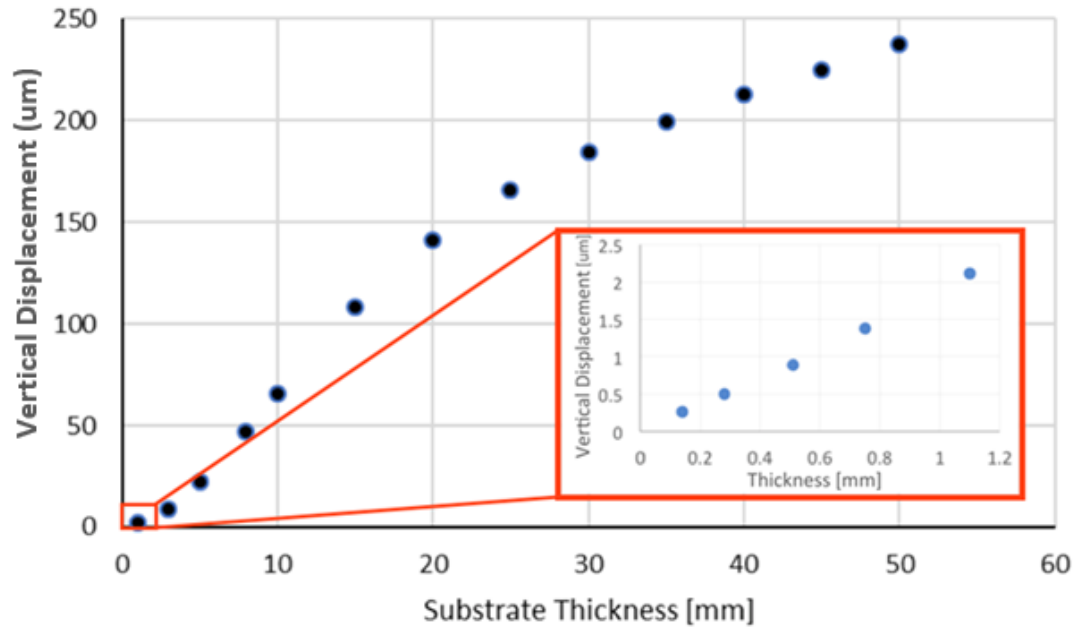


Figure 16: Max vertical displacement at the ice-PDMS interface as a function of PDMS thickness. These values were from the FEM analysis.

Table 6: The effect of PDMS thickness on max displacement and ratios between horizontal and vertical displacements. These values were from the FEM analysis.

Surface Thickness (mm)	Vertical Displacements (μm)	Horizontal displacements (μm)	Horizontal: Vertical Displacement	Vertical: Horizontal Displacement
0.14	0.26	5.57	21.43	0.05
0.28	0.50	10.97	21.94	0.05
0.51	0.89	19.48	21.92	0.05
0.75	1.38	27.82	20.19	0.05
1	1.89	36.46	19.33	0.05
1.1	2.113	39.78	18.82	0.05
3	8.74	93.52	10.70	0.09
5	22.12	137.09	6.20	0.16
8	46.95	189.20	4.03	0.25
10	65.38	219.22	3.35	0.30
15	107.95	288.69	2.67	0.37
20	141.35	357.01	2.53	0.40
25	166	426.11	2.57	0.39
30	184.45	497.57	2.70	0.37
35	199.48	573.22	2.87	0.35
40	212.60	654.55	3.08	0.32
45	224.98	742.7	3.30	0.30
50	237.22	838.57	3.53	0.28

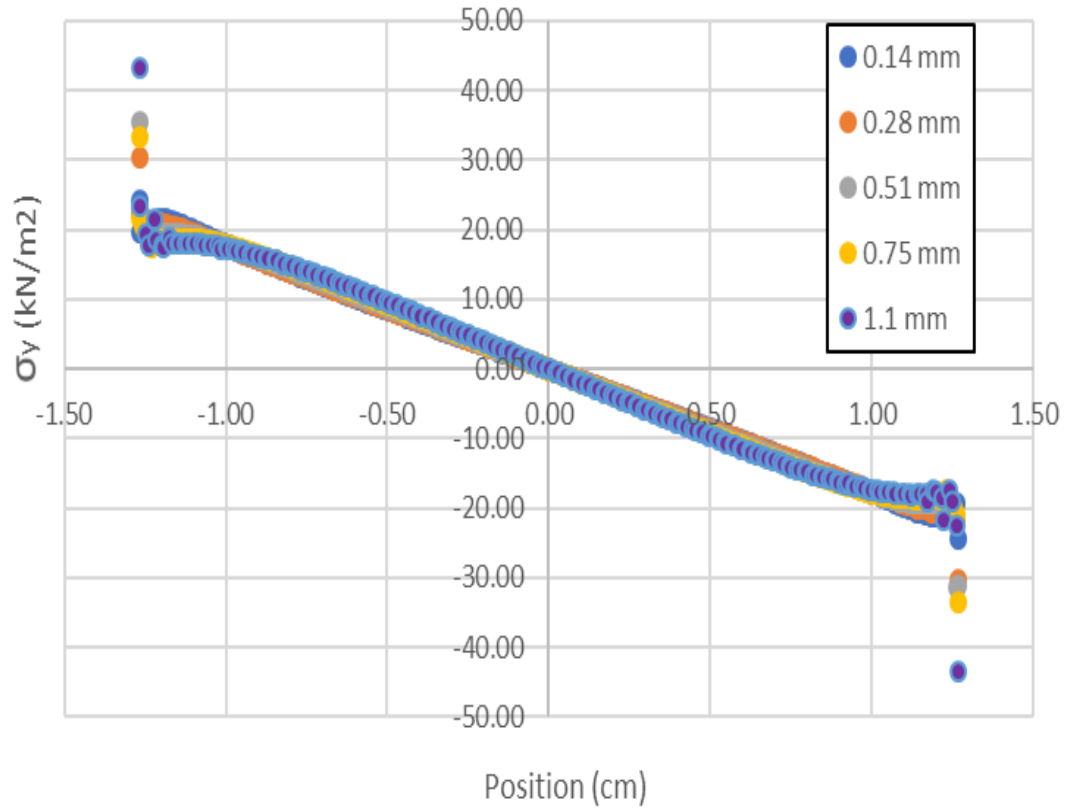


Figure 17: Distribution of normal stresses (the peeling stresses) across the ice/substrate interface for increasing substrate thicknesses. These values were from the FEM analysis.

Figure 18 shows the vertical displacement along the interface between the ice block and a PDMS surface. The vertical displacement profile was taken from the edge where the pressure was applied to the center of the ice block. The vertical displacement is maximum at the edge of the ice block and zero in the center. The vertical displacement also decreases in a linear manner from the edge to the center. Figure 19 presents the vertical displacement along the interface between the ice block and a polycarbonate surface. The vertical displacement of the ice-substrate interface was about 300-fold lower on the polycarbonate surface than on the PDMS surface. The curve also decreased more exponentially than linearly. Figure 20 shows the vertical displacement along the interface between the ice block and a steel surface. The vertical displacement along the interface further decreased in the steel model, with the vertical displacements in the steel models being approximately 2-fold lower than polycarbonate model and 600 times lower than the PDMS model. The vertical displacement also decreased approximately exponentially from the edge to the surface center. The steel substrate was the stiffest of the three surfaces and the PDMS surface was the softest surface, see Table 3 in the methods.

Figure 21 shows the max vertical displacement at the ice-substrate interface. The 3 mm thick sample exhibited the vertical displacement decreasing by approximately 550-fold as the substrate stiffness increased from 750 kPa to 50 GPa. The 8 mm thick substrate generated the vertical displacement decreasing by approximately 2800-fold. Therefore, it can be concluded that the max vertical displacement decreases as the Young's modulus increases for both thicknesses. However, the displacements for the thicker sample were higher for a given stiffness and the curve was much steeper than for the thinner sample.

Furthermore, the max horizontal displacement at the interface decreased by approximately 3400-fold for the 3 mm thick substrate as the substrate stiffness increase from 750 kPa to 50 GPa. For the 8 mm thick substrate, the max horizontal displacement decreased by approximately 6200-fold. Table 7 presents the 3 mm max horizontal displacements for the 3 mm thick substrate, max vertical displacements, and the ratios between them as a function of substrate stiffness. Table 8 lists the 8 mm substrate's max horizontal displacements, max vertical displacements, and the ratios between them.

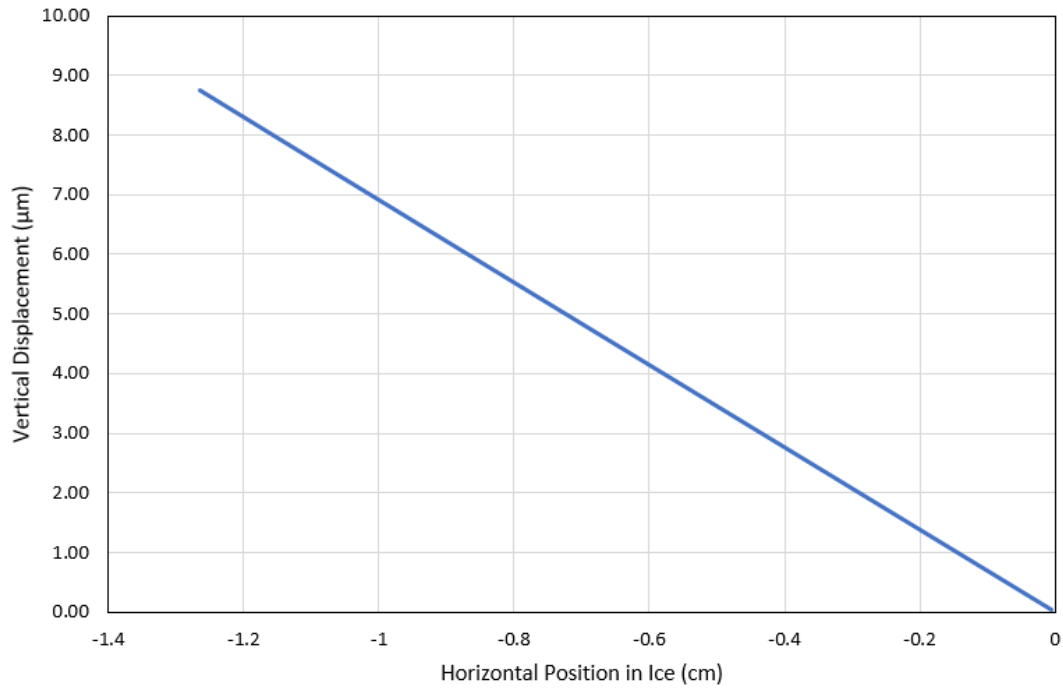


Figure 18: Vertical displacements across the ice/substrate interface from the pressurized edge to the center of the ice for a PDMS substrate. These values were from the FEM analysis.

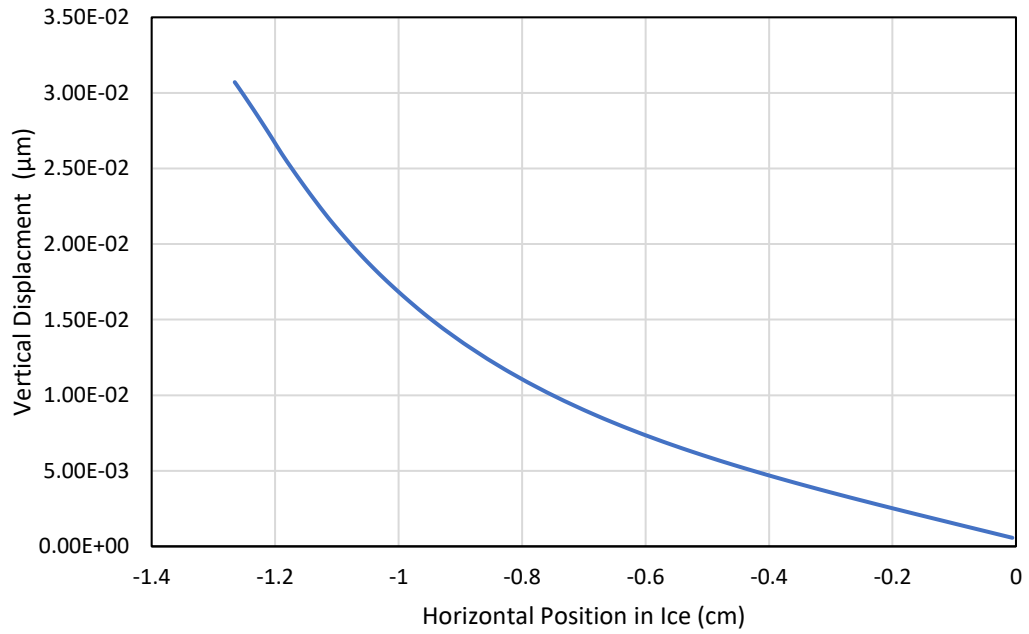


Figure 19: Vertical displacements across the ice/substrate interface from the pressurized edge to the center of the ice for a polycarbonate substrate. These values were from the FEM analysis.

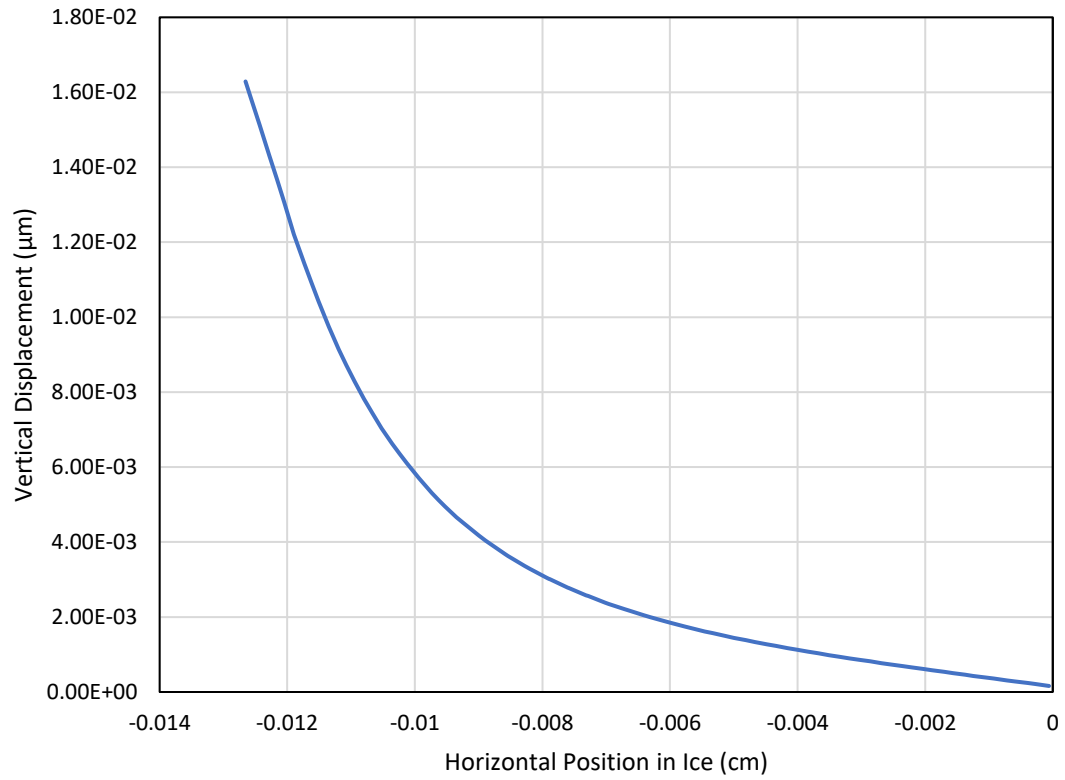


Figure 20: Vertical displacements across the ice/substrate interface from the pressurized edge to the center of the ice for a steel substrate. These values were from the FEM analysis.

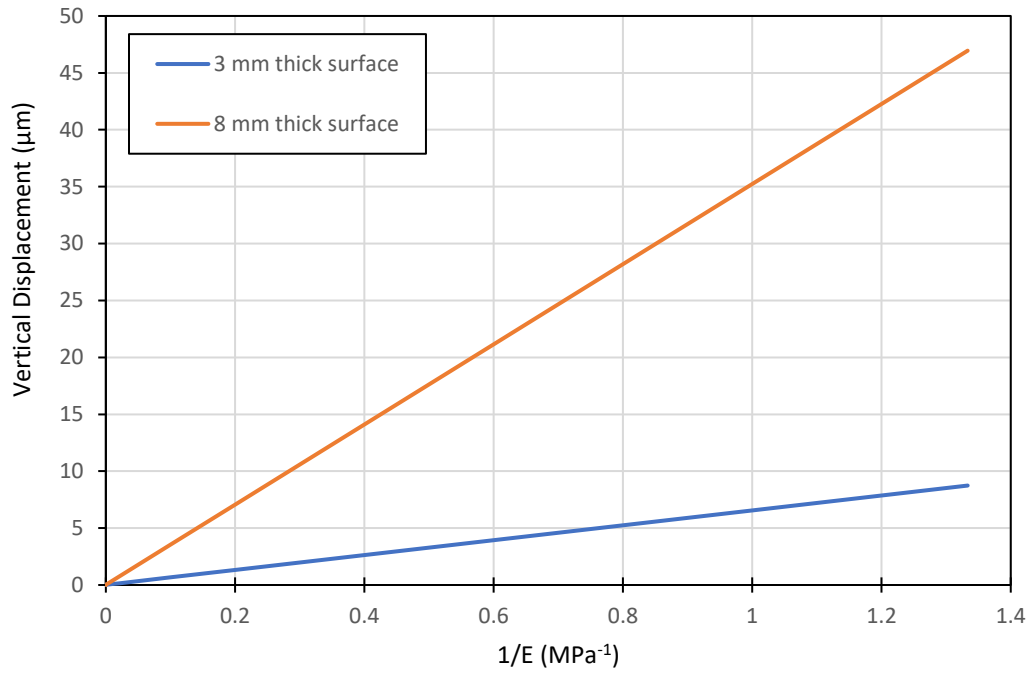


Figure 21: Max vertical displacement at the ice/substrate interface as a function of inverse substrate stiffness. The substrate thickness was set to 3mm and 8mm, respectively. These values were from the FEM analysis.

Table 7: The effect of substrate stiffness on max displacement and ratios of horizontal to vertical displacements for the 3mm thick substrate. These values were from the FEM analysis.

Substrate stiffness (mPa)	Vertical Displacements (μm)	Horizontal Displacements (μm)	Horizontal: Vertical Displacement	Vertical: Horizontal Displacement
0.75	8.738	93.522	10.703	0.093
1	6.555	70.149	10.702	0.093
5	1.326	14.056	10.600	0.094
10	0.67283	7.0439	10.469	0.096
50	0.14962	1.4343	9.586	0.104
100	0.0841505	0.73303	8.711	0.115
500	0.031338	0.17142	5.470	0.183
1000	0.024405	0.10074	4.128	0.242
5000	0.018146	0.043023	2.371	0.422
10000	0.017172	0.035454	2.065	0.484
50000	0.016388	0.029185	1.781	0.562
100000	0.016166	0.02838	1.756	0.570
500000	0.016065	0.027731	1.726	0.579

Table 8: The effect of substrate stiffness on max displacement and ratios of horizontal to vertical displacements for the 8mm thick substrate. These values were from the FEM analysis.

Substrate stiffness (mPa)	Vertical Displacements (μm)	Horizontal Displacements (μm)	Horizontal: Vertical Displacement	Vertical: Horizontal Displacement
0.75	46.95	189.2	4.03	0.25
1	35.225	141.91	4.03	0.25
5	7.058	28.407	4.02	0.25
10	3.537	14.219	4.02	0.25
50	0.7205	2.8691	3.98	0.25
100	0.36844	1.4502	3.94	0.25
500	0.08685	0.3148	3.62	0.28
1000	0.0517045	0.17255	3.34	0.3
5000	0.02352	0.057725	2.45	0.41
10000	0.019894	0.042935	2.16	0.46
50000	0.016852	0.030724	1.82	0.55

Discussion

The wedge model suggests that the results will vary depending on whether ice forms under the mold or not. If ice forms underneath the mold, then the displacements will be similar to the case in which the ice is without a mold. However, if the gap between the PDMS surface and the mold is left empty then the vertical displacements will increase by approximately 50-80%, depending on the gap size. The steel mold in the model was also changed to polycarbonate (data not shown), but the results were not significantly different.

The fact that higher vertical displacements are generated by the empty gap implies that the ice should experience higher peeling forces, specifically on the side in which the force is applied, and thus higher normal stresses. For the ideal ice adhesion test there should not be any normal stresses or peeling at the ice/substrate interface. The idea behind the ice adhesion test is to measure the forces needed to shear the ice from the surface. Thus, the empty gap between the mold and substrate is highly detrimental to the test. The vertical displacements decreased after the gap became bigger than 1° , which implies that small gaps (almost like sharp cracks) are more detrimental to the ice adhesion test than larger gaps. However, as alluded to earlier, the best situation is to avoid any gaps under the mold by either filling them with ice or by removing the mold.

The piston position models show that the vertical displacements increase as the piston is moved to higher positions. This is reasonable because pushing the ice from the top should produce more torque than pushing the ice from the bottom, thus creating a larger rotation of the ice. The piston models also illustrate that the easiest way to minimize vertical displacements is to have the piston positioned as close as possible to the substrate. Though

there is a limit to how low the piston can be placed before it starts to drag against a substrate. Also, there will always be some vertical displacements due to substrate deforming during the test. Thus, the Ling et al. ice adhesion test [21] will result in some vertical displacements especially for soft materials due to its configuration, and thus a pure shear stress condition cannot be generated. However, the Ling et al ice adhesion test [21] can be optimized by minimizing the vertical displacements. In this research the piston was kept at 3 mm above the substrate's surface to minimize torque and vertical displacement, and to keep the piston from dragging

The thickness models showed that the displacements at the ice-PDMS interface increased as the thickness increased. However, the change in the displacements became less drastic for the thicker models. The decreasing slope of the thickness-displacement curve (Fig. 16) could be caused by changes in geometry and rotation of the ice. For examples, it is possible that after a certain thickness the PDMS on the right side, the side being embedded, starts to apply higher normal forces to the right edge of the ice and thus starts to counteract the rotation of the ice.

The normal stresses in the thickness models showed that the stresses at the edges increased as the substrate thickness increased. The mesh density along the interface did not change between thickness models to minimize edge affect. Such a change would cause the stresses at edges to increase as the mesh density increases. Thus, the only thing changing in the models was the substrate thickness. The changes in vertical displacements are likely responsible for the changes in normal stresses. The thicker materials had higher vertical displacements and caused higher lifting of the left edge; which in turn would cause more

stress at the interface because the PDMS is being stretched. The normal stresses also suggest that the left edge is likely the failure point at which the ice begins to detach from the PDMS.

The final set of models shows that the stiffness of the substrate has a profound effect on the displacements. The stiffness models implied that the softer substrate materials had higher displacements than more rigid materials for samples of the same thickness. The vertical displacements on a PDMS surface was approximately 6000 times greater than on polycarbonate. Thus, the stiffness models imply that normal stresses on the edge will be greater for softer materials, like PDMS, than for rigid materials, like polycarbonate. Varying the thickness in these models also revealed that stiffness has less of an effect on displacements when the substrate is thin. Therefore, these thinner samples should be used to minimize the stiffness effect. It should be noted that vertical displacement from the ice edge to the ice center should have decayed exponentially, rather than linearly, for each of the substrates. The linear decay in the PDMS substrate model is most likely caused by computational error due it being treated as a linear elastic material rather than a hyper-elastic material.

Chapter Three: Experimental Evaluation of Mold Type and Substrate Thickness on Ice Adhesion Testing

Introduction

Ice adhesion tests were performed on PDMS samples with three different mold types and several substrate thicknesses. Initially, a steel mold was used to form the ice cube. However, the steel mold could not be removed before the ice adhesion test without severely damaging the ice samples. To improve the test, Monika Bleszynski suggested using a mold made of PDMS which could be removed before testing [27]. A third mold made of polycarbonate was also used during the test. The polycarbonate mold was not removed before the ice adhesion test because attempts to remove it would result in the debonding of the ice from the sample. The test apparatus used in the experiments below was designed by Dr. James Middleton and was based on the Ling et al. test apparatus [21]. The substrate thickness effect was evaluated by producing five samples of various thicknesses.

Methods

Ice was adhered to DragonSkin 20 (Smooth-On, Inc.) in all the experiments discussed below. DragonSkin 20 is a commercial platinum catalyzed PDMS based silicone

rubber. DragonSkin is a low surface energy material, soft (20A on the shore A hardness scale), and has a density of 1.08 g/cm^3 . DragonSkin is a two-part silicone rubber, in which part A consist of uncross-linked PDMS chains, while part B consists of the crosslinker agent and the platinum catalyst. Parts A and B were mixed in a 1 to 1 ratio to produce a fully cross-linked sample. The DragonSkin solution was poured onto a glass slide and placed into an Ossila Spin Coater. The samples used to evaluate the mold effect were spun at 500 RPMS for 60 seconds, which corresponded to a sample thickness of 0.51mm. The samples were then left in the spin coater for at least 4 hours to solidify and then placed in storage overnight to completely cure. Figure 22 shows the spin coater, cold plate, and the test apparatus. Figure 23 presents a schematic of the ice adhesion test.

Samples were fastened to a Peltier cold plate (made by TE technology, Inc.) and a mold was placed on top of the samples. A layer of water was then pipetted into the mold. The initial volume of water was minimized to prevent leaking. The cold plate was then cooled to $-10 \text{ }^\circ\text{C}$ and maintained using a thermoelectric temperature controller (TE Technology, Inc. TC-48-20). More water was added to the mold after the initial layer was frozen and styrofoam insulation was placed over the cold plate during the freezing process. The larger molds were filled to approximately 50% and the smaller molds were filled to approximately 75% of their total volume. Typically, it took about 2 hours to completely form the ice block.

The steel and polycarbonate molds used in the ice adhesion experiments were purchased from McMaster-Carr and cut down to be about an inch tall. The steel mold had an inner surface area of 44 mm^2 molds and the polycarbonate mold had an inner surface of

49 mm². Monika Bleszynski produced a PDMS mold by coating the outside of a polycarbonate square tube with an RTV-1 (one component) silicone rubber. The polycarbonate tube had a Teflon tape on the outside of it to prevent the PDMS from sticking. The PDMS mold was given a few days to fully cure. The fully cured PDMS mold had an inner area of 63 mm². Figure 24 shows the molds used in the research.

During the ice adhesion test, a piston attached to a force sensor (Series 5 mark-10) was pushed against the ice block. The styrofoam insulation was removed from the cold plate before the ice adhesion experiment took place. The force sensor was suitable up to 250 N and had a sensitivity of ± 0.01 N, respectively. The sensor was attached to a linear stage (Newmark Systems, Inc.), which moved at speeds of 0.025 mm/sec during the experiment. The max force required to dislodge the ice was recorded using the program MESUR Lite by Mark-10. The ice adhesion strength was then calculated using equation 1.

The test was then further adjusted to better represent the Fu et al. test [22] by sealing the bottom of both the steel and polycarbonate molds using RTV-1 and parafilm. The cold plate was placed in a chest freezer, with the temperature set to approximately -10 °C, and then the sealed molds were placed on top of the cold plate. The molds were then filled to the brim with water. The PDMS samples were then placed on top of the molds and positioned to be in contact with the water. The samples were left in the freezer until the water froze, then flipped and fastened to the cold plate. The linear stage was then moved to the deep freezer and the ice adhesion test was subsequently performed within the freezer.

PDMS samples with various thicknesses were also produced to investigate the thickness effect on the ice adhesion results. The thicknesses were changed by spin coating

samples at different speeds, while keeping the spin time constant at 60 seconds. The speeds of the spin coater were 100, 150, 250, 500, and 1000 rpms. This corresponded to sample thicknesses of 0.14 mm, 0.28 mm, 0.51 mm, 0.75 mm, and 1.1 mm; with samples thicknesses decreasing as the rpms increased. The removable PDMS molds were used to form the ice block adhered to the sample substrate and each sample was given at least 24 hours to cure before undergoing a test. Each of the tests was performed on the cold plate outside of the chest freezer.



Figure 22: Cold plate with ice adhesion test apparatus (left) and spin coater (right).

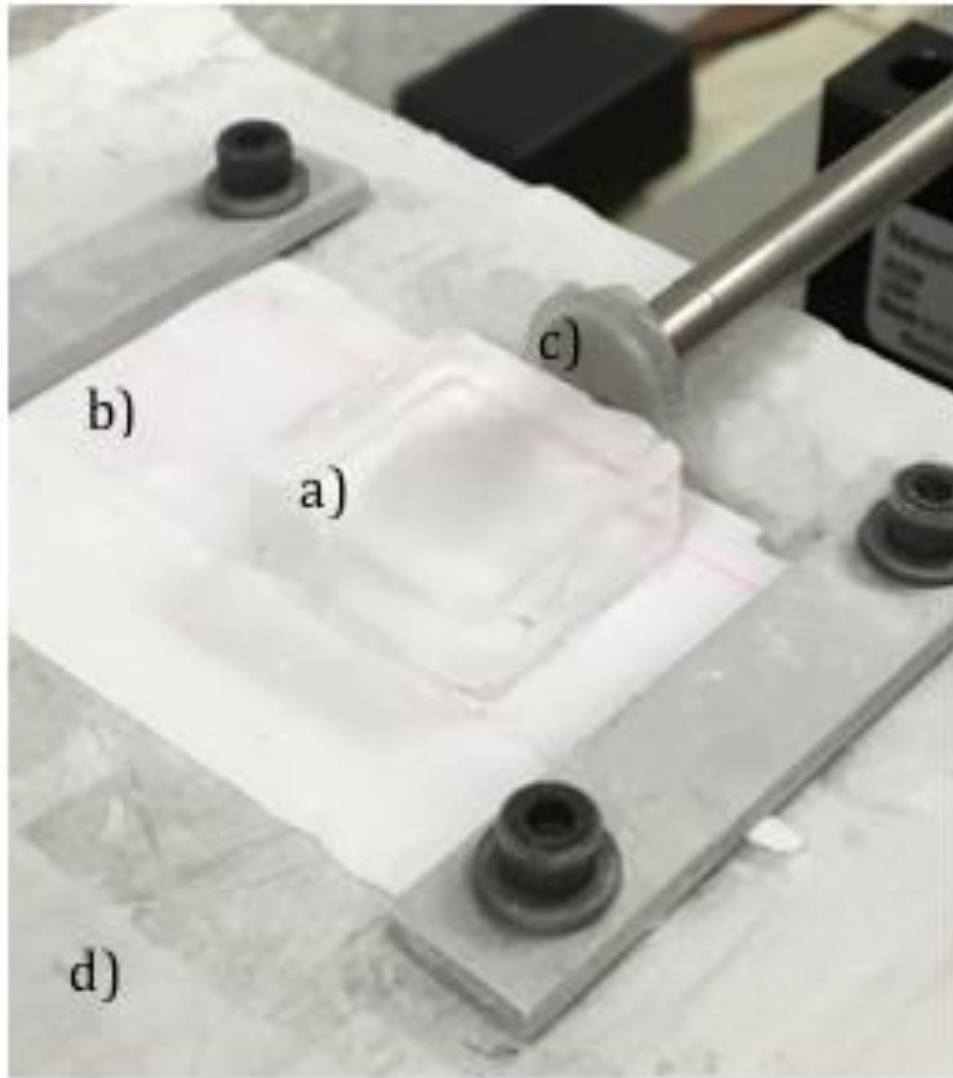


Figure 23: photo of the ice adhesion test (a) the ice block, (b) PDMS substrate on glass slide, (c) push-rod coated with PDMS, and (d) cold plate.

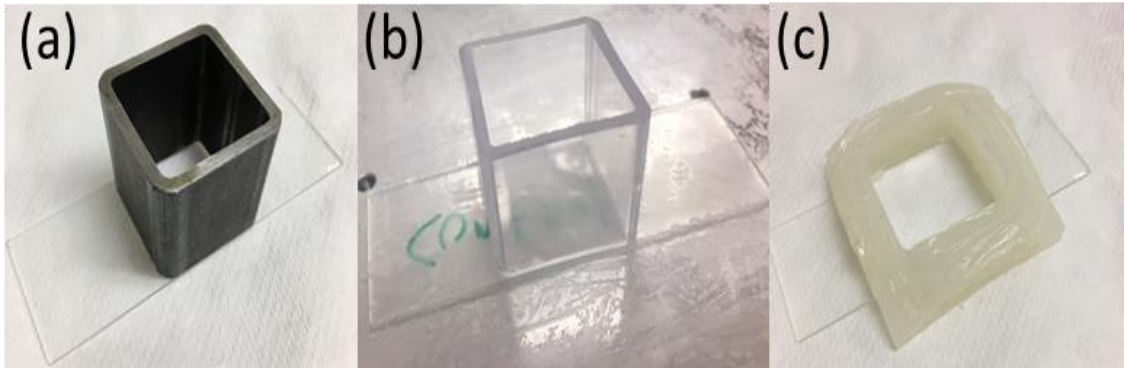


Figure 24: (a) steel, (b) polycarbonate, and (c) PDMS molds used to form ice cubes for the ice adhesion tests. Only the PDMS mold was removed prior to the test.

Results

Figure 25 shows the results for the ice adhesion test using sealed and unsealed molds. The test using the unsealed molds is referred to as the standard test and the test using the sealed mold is referred to as the inverted test. These results were based on 5 ice adhesion tests for each mold. The ice adhesion strengths varied greatly depending on the type of mold used in the standard test and on whether the mold was removed or not. Removing the PDMS mold from the 0.51 mm thick samples produced the highest average ice adhesion strength with 24.06 kPa, followed by polycarbonate with 13.86 kPa. The steel mold produced the lowest average adhesion strength with 9.56 kPa. These values were based on 5 tests were performed with each mold. This corresponded to the removable mold producing an ice adhesion strength 2.5 times higher than the steel mold and the polycarbonate mold producing an ice adhesion strength 1.4 times higher than the steel mold. However, the scatter for the PDMS was much greater than for either the steel or the

polycarbonate molds. The test without a mold produced a scatter of ± 4.20 kPa, whereas the polycarbonate produced a scatter of ± 2.94 kPa. The steel produced the lowest scatter of ± 1.73 kPa. The scatter was determined using the standard deviation among samples of the same thickness.

The ice adhesion strengths for the inverted test were higher than the standard test. The average ice adhesion strength for the steel mold test increased to 12.67 kPa and the strength for the polycarbonate mold increased to 16.62 kPa. The scatter was also slightly lower for the inverted test than for the standard test, with the scatter for the steel mold being ± 1.02 kPa and the polycarbonate mold having a ± 1.95 kPa scatter. There was also a noticeable gap seen between the ice sample and mold when the inverted test took place. The gap was noticeable in both the polycarbonate mold and the steel mold. Figure 26 shows the gap seen after the water frozen in the sealed steel mold and the sealed polycarbonate mold.

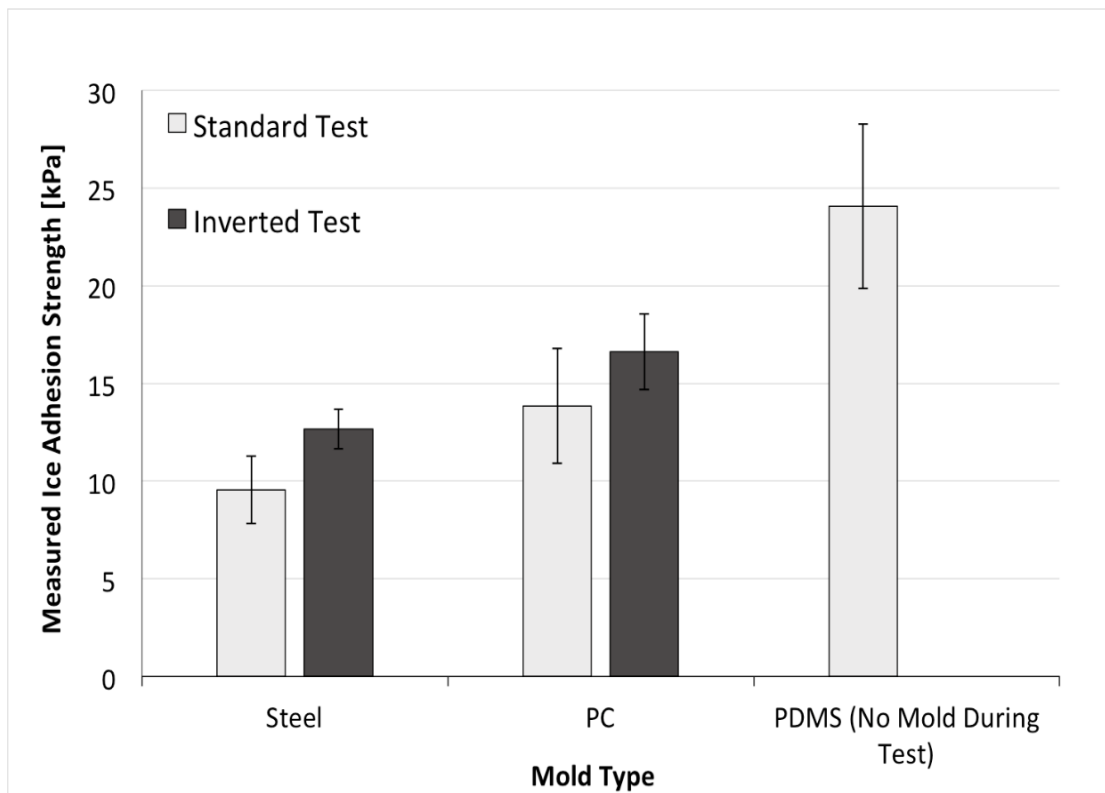


Figure 25: Ice adhesion strength for steel, polycarbonate, and removable PDMS molds. The substrate PDMS film samples were 0.51 mm thick. 5 tests were performed with each mold for the inverted and standard test.

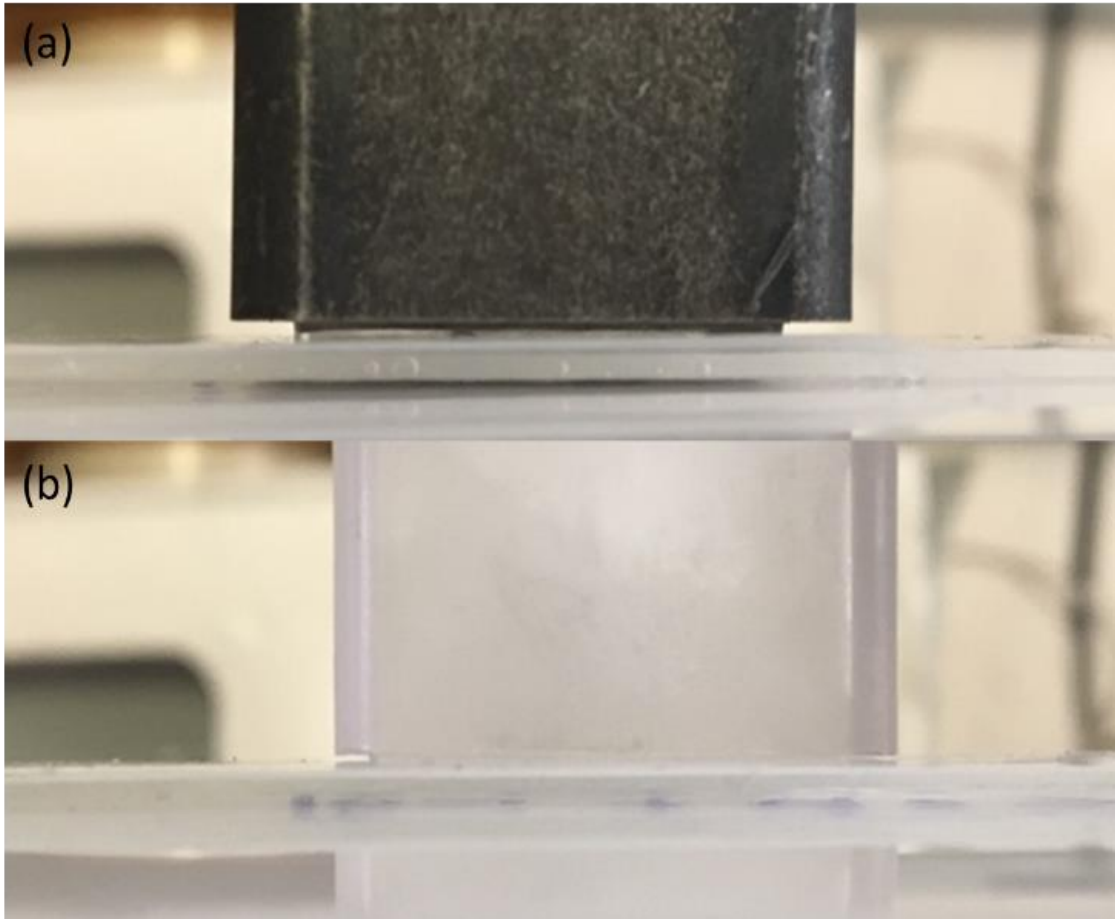


Figure 26: Sealed steel (a) and polycarbonate (b) molds after freezing. Gap formed between the molds and the sample in both cases.

Figure 27 presents the ice adhesion strength for the various substrate thicknesses. These values were determined from 5 independent tests. The highest ice adhesion strength (32.16 ± 4.94 kPa) was obtained from the 0.14 mm thick sample and the lowest strength from the 1.1 mm thick sample (11.77 ± 2.50 kPa). The 0.28 mm thick sample resulted an ice adhesion strength of 24.06 ± 4.20 kPa, the 0.51 mm sample exhibited an adhesion strength of 17.55 ± 1.37 kPa, and the 0.75 mm sample resulted in an adhesion strength of 12.41 ± 3.38 kPa, See Table 9. Thus, the highest ice adhesion strength was obtained from the thinnest sample, and the ice adhesion strength decreased as the sample thickness increased. However, the change in ice adhesion strength due to increasing thickness began to plateau after the sample became thicker than 0.75 mm. Thus, increasing the thickness further should have a negligible effect on the ice adhesion strength. This observation is consistent with the results reported by other research groups studying the effects of ice adhesion on soft rubbers [3, 4]. A linear trend line was then used to determine the ice adhesion strength for a ‘zero-thickness’ sample. The trend line was applied to the first four thicknesses because the ice adhesion strength changed linearly in this region. The linear trend line suggests that the ‘zero-thickness’ sample should produce an ice adhesion strength of 34.63 kPa.

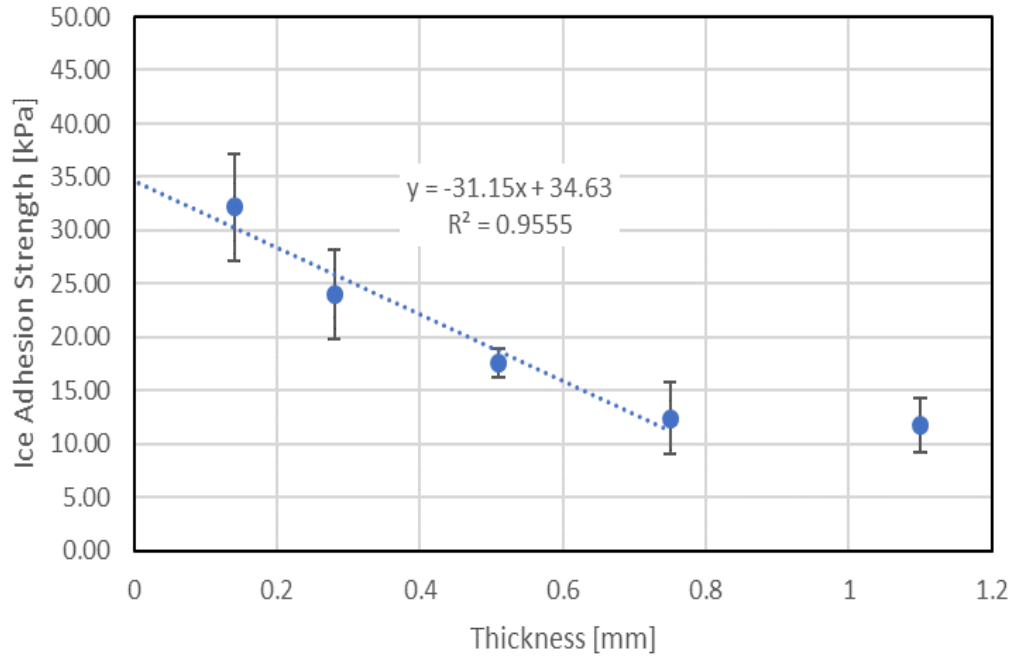


Figure 27: Ice adhesion strength as a function of sample thickness. 5 tests were performed for each thickness.

Table 9: Ice adhesion strength as a function of sample thickness. The Scatter was determined using the standard deviation.

Sample Thickness [mm]	Ice Adhesion Strength [kPa]
0.14	32.16 ± 4.94
0.28	24.06 ± 4.20
0.51	17.55 ± 1.37
0.75	12.41 ± 3.38
1.1	11.77 ± 2.50

Discussion

The results produced by using of the steel, polycarbonate, and removable PDMS molds were significantly different. The ice adhesion strength was highest when the mold was removed, which implies that removing the mold did not cause any debonding between the ice and the substrate. The lowest ice adhesion strength was seen when the steel mold was used, and the usage of the polycarbonate molds produced an ice adhesion strength slightly above that of the steel mold. It should be noted that examining of the steel mold after the ice adhesion test showed that ice did not form on the bottom of the steel mold. This indicated that water did not leak underneath of the steel mold. This also implies that it was reasonable to assume that an empty gap formed between the mold and the substrate as previously illustrated in the FEM section. The lower ice adhesion for the steel mold compared to the removable mold also provides some validity to the FEM analysis. The FEM model of the steel mold had larger vertical displacements than the ice block model, which would cause the ice to experience a larger peeling force. Thus, the ice would be easier to remove because it is easier to peel apart two objects than to shear them apart. It is also possible that the gap acts as a miniature crack, which would cause larger stress to concentrate on the edge of the ice and thus making it easier to dislodge it from the sample. The increase in ice adhesion during the inverted test can also be explained using the wedge models. The vertical displacements in the wedge models initially decreased after the wedge was enlarged from a 0.1° to a 1° gap. If the vertical displacements decrease then the peeling force should also decrease; thus, making harder to dislodge the ice and increasing the amount of force needed to break apart the surfaces.

However, the FEM models cannot explain the discrepancies between the polycarbonate and the steel molds. It was observed that the ice formed in the steel mold appeared to have more dendrites than the ice formed in the polycarbonate mold, or the removable PDMS mold. It is possible that the crystalline microstructure of the ice was affected by cooling rates or by different intermolecular interactions between water and the molds. This could have affected the microstructure of the ice and its adhesion strength to the PDMS surface. Parameters that affect the ice crystalline structure need to be further investigated though before this claim can be verified.

Finally, the thickness test showed that adhesion strength decreased with increasing thickness. This again was consistent with the results from the FEM analysis. The FEM thickness models showed that the vertical displacements increased as the sample thickness increased. Thus, the peeling force should increase as the sample become thicker and therefore it should be easier to remove the ice. The ice adhesion strength at the “zero-thickness” was then determined using a trendline because the “zero-thickness” would be the point at which thickness ceased to affect the ice adhesion strength. The ice adhesion at the “zero-thickness” would be closer to the real adhesion strength between the ice and the DragonSkin. This method was favored because attempts to perform ice adhesion tests on thinner samples produced unreliable results. For example, ice adhesion tests were performed on 0.1 mm thick substrates (data not provided). The very thin substrates would tear and detach from the glass slide during the test which caused the results to be highly variable and inaccurate. Thus, it was decided that a trendline could be used to extrapolate

the ice adhesion strength to zero thickness. The trend line was also used to develop a thickness correction factor that could be used for DragonSkin.

Chapter Four: Effects of Crosslink Density and Aging of PDMS Substrates on Ice Adhesion

Introduction

The final set of experiments involved varying the crosslink density in PDMS to evaluate its effect on the ice adhesion strength. It has been reported in the literature that varying the crosslink density in elastomers changes their ice adhesion strength [3, 4]. DragonSkin samples with varying degrees of crosslink density were produced by varying the amount of crosslinker. The ice adhesion strengths were then measured for the samples. Samples with varying crosslink density were then aged to determine if their ice adhesion properties would change. Hypochlorous acid was used to accelerate the aging of samples. Monika Bleszynski has previously shown that hypochlorous is extremely damaging to silicone rubbers and can be used to accelerate their environmental aging [28]. The aged samples were then examined for damage and their ice adhesion strength was tested.

Methods

The DragonSkin samples were created by reducing the amount of crosslinking agent and catalyst by 25%, 50%, and 75%. The samples were then spin coated at 500 rpms for 60 seconds and given 24 hours to fully cure before testing. Five samples were produced

for each crosslink density. The removable PDMS mold was used to form the ice. The ice adhesion strengths were also corrected to negate the thickness effect. The reduced crosslinked samples were then aged by soaking them in hypochlorous acid (Blue-LYTE). Five samples for each crosslink density were placed in a 1000 mL beaker and submerged in a 0.046% hypochlorous acid solution at a concentration of 500 ppm of free chlorine; resulting in a 0.05% total chlorine concentration. The top of the beaker was sealed with parafilm to minimize the evaporation of the hypochlorous acid solution. The acid was maintained at room temperature for a duration of 4 weeks. The samples were given 3 days to dry in air at room temperature after removal from the hypochlorous acid aging. The samples were weighed before and after aging. Their ice adhesion strengths were determined, and the strengths were also corrected to negate the thickness effect.

Results

Table 10 lists the ice adhesion strengths for the various crosslinked PDMS samples. The highest ice adhesion strength was seen in the normal crosslink sample; with an ice adhesion strength of 36.63 ± 6.05 kPa. The 25% reduced sample exhibited an ice adhesion strength of 24.6 ± 6.10 kPa; which corresponded to a 32.84% reduction in the ice adhesion strength from the fully crosslinked sample. The 50% reduced sample exhibited an ice adhesion strength of 21.0 ± 7.53 kPa; which resulted in the ice adhesion strength being 42.67% lower than the fully crosslinked sample. The lowest ice adhesion strength was observed in the 75% reduced crosslink sample; with an ice adhesion strength of 17.4 ± 3.97 kPa. The 75% reduced samples resulted in the ice adhesion strength dropping by 52.50%

in comparison with the fully crosslinked sample. Thus, the ice became easier to dislodge from the sample as the crosslink density decreased. It should be also noted that the 75% reduced sample felt tacky when touched. The ice adhesion strength was determined by performing 5 tests for each of the crosslink densities. The scatter was determined using the standard deviation among samples of the same crosslink density.

Table 10: Ice adhesion strength of Dragon Skin RTV-2 as a function of cross-linker agent. 5 tests were performed for each crosslink density.

Crosslink Density of PDMS	Ice Adhesion Strength [kPa]
100%	34.63 ± 6.05
75%	24.6 ± 6.10
50%	21.0 ± 7.53
25%	17.4 ± 3.97

Table 11 presents the sample mass lost caused by the aging whereas Table 12 lists the ice adhesion strengths for each crosslink density after aging. The 100% crosslinked samples exhibited a loss $0.37 \pm 0.27\%$ of its total weight after aging, whereas the 25% reduced samples lost $0.88 \pm 0.52\%$ of their total weight. The 50% reduced samples lost $0.16 \pm 0.11\%$ of their total weight and the 25% reduced samples lost $0.64 \pm 0.48\%$ of its weight. Thus, the 25% and 75% reduced samples tended to lose more mass than the normal samples or the 50% reduced. However, the standard deviation for mass lost was high for each of the crosslinked densities. Thus, the only results that can be inferred from weighing the samples is that the samples appeared to be damaged due to their mass lost.

The highest ice adhesion strength was observed in the 25% reduced samples with an ice adhesion strength of 49.74 ± 3.75 kPa. This was comparable with the normal crosslink sample, which had an ice adhesion strength of 46.67 ± 2.60 kPa. The 75% reduced sample fared slightly better with an ice adhesion strength of 46.51 ± 1.87 kPa, but it too lost its low ice adhesion when compared to the normal crosslinked sample. The 50% reduced sample fared the best with an ice adhesion strength of 36.57 ± 5.58 kPa, which is comparable with the ice adhesion strength of the normal sample before aging. The ice adhesion strength was determined by performing 5 tests for each of the crosslink densities. The scatter was determined using the standard deviation among samples of the same crosslink density.

It should be noted that the sample color changed after being aged in hypochlorous acid. The DragonSkin samples are normally clear, but the aged samples became opaque. Figure 28 shows the 100% crosslinked samples before and after aging. Figure 29 shows that the normal, 25% reduced, 50% reduced, and 75% reduced samples after aging.

Table 11: Mass lost caused by aging for the 100%, 25%, 50%, and 75% reduced crosslinked samples.

Sample #	Loss of Mass (%)			
	Control	25% reduced	50% reduced	75% reduced
1	0.34	1.17	0.35	0.37
2	0.69	1.63	0.07	1.50
3	0.10	0.71	0.17	0.49
4	0.59	0.30	0.11	0.34
5	0.13	0.59	0.10	0.52
Average	0.37 ± 0.27	0.88 ± 0.52	0.16 ± 0.11	0.52 ± 0.48

Table 12: Ice adhesion strengths of Dragon Skin RTV-2 after aging in hypochlorous acid for 4 weeks. 5 tests were performed for each crosslink density.

Crosslink Density of PDMS	Ice Adhesion Strength [kPa]	Increase in Ice Adhesion strength from un-aged sample (%)
100%	46.67 ± 2.60	34.8
75%	49.74 ± 3.75	102.2
50%	36.57 ± 5.58	74.1
25%	46.51 ± 1.87	167.3

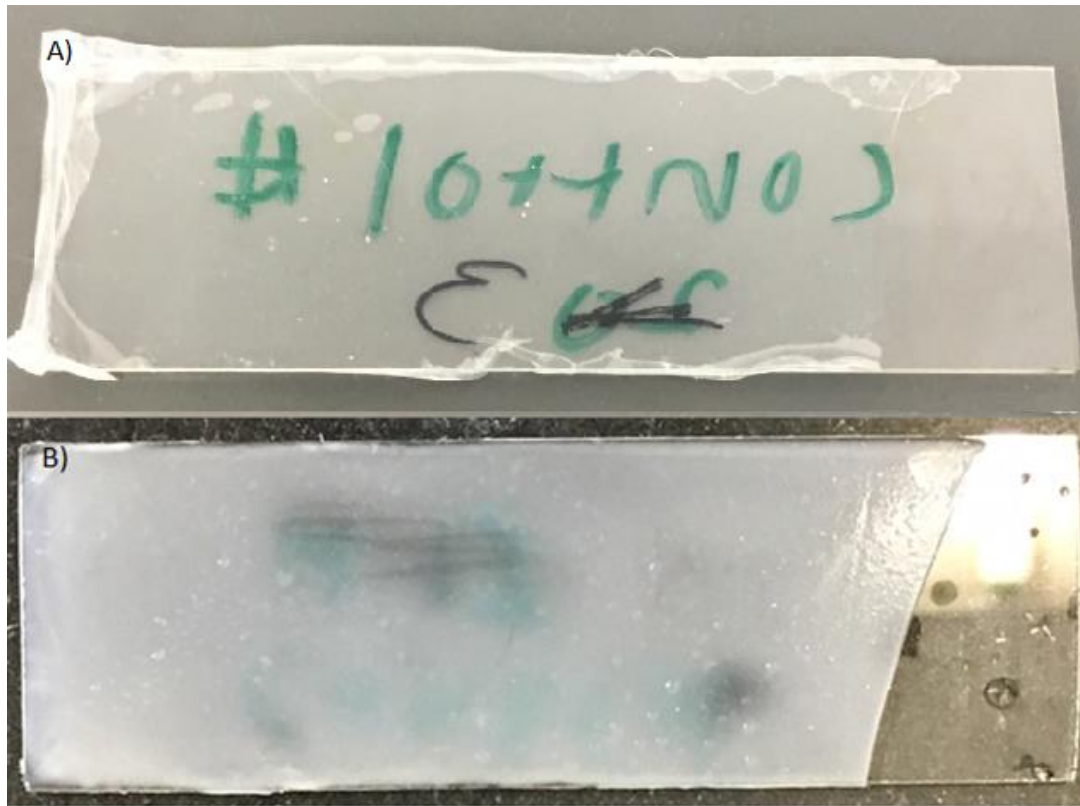


Figure 28: Normal crosslinked Dragon skin sample (A) before aging and (B) after being aged in hypochlorous acid for 4 weeks.

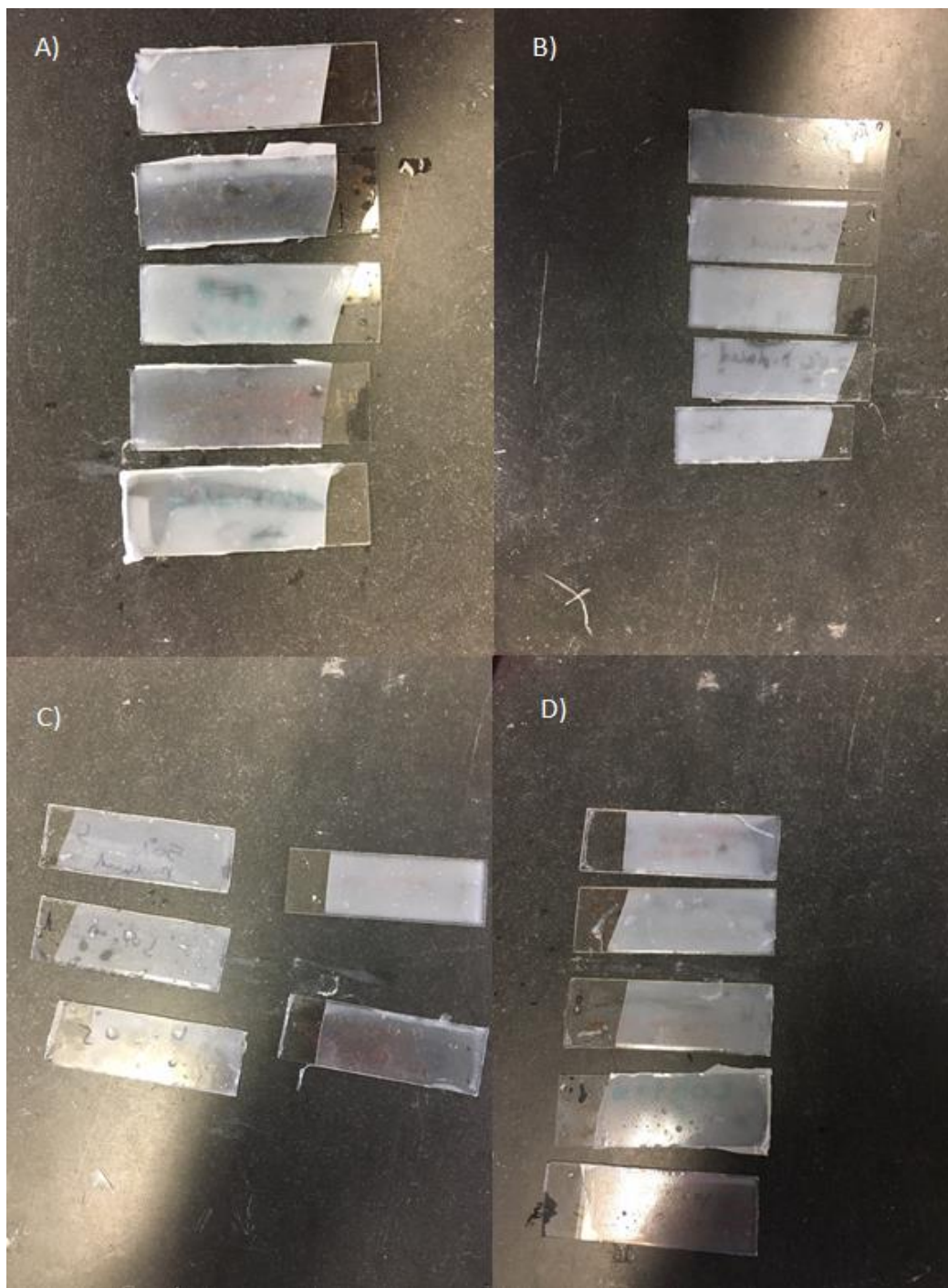


Figure 29: (A) 100%, (B) 25% reduced, (C) 50% reduced, and (D) 75% reduced crosslinked samples after aging.

Discussion

The experiments showed that the ice adhesion strength decreased as the crosslink density decreased. The two possibilities for the changes in ice adhesion strength are either that lowering the crosslink density caused the material to become softer or that the reduction in crosslinker agent resulted in some uncross-linked PDMS chains forming a lubricated layer on the surface. The stiffness related FEM models showed that softer materials of the substrates exhibited higher vertical displacements than harder materials, which would increase the peeling force, making easier to dislodge the ice from the PDMS.

Limited hardness tests were performed on the samples (data not shown here) with their hardness dropping from 20 A for the fully crosslinked sample to 18A for the 25% reduced samples on the shore hardness A scale. Therefore, some of the changes in ice adhesion should be caused by the change in hardness. However, the 75% reduced samples also had a tacky feel to it. This implies that not all the PDMS chains were fully crosslinked. It is also possible that low molecular weight chains, or shorter chains, formed a layer on the surface. This could form a lubricating layer between the ice and the PDMS surface like the SLIP material mentioned in Chapter 1, which would cause the ice adhesion strength to decrease. Thus, it is possible that the decrease in the ice adhesion strength of the partially cross-linked samples was caused by a combination of changes in the materials hardness and by the formation of a low molecular chain lubricating layer.

Aging of the various crosslinked DragonSkin samples showed that the initial benefit caused by lowering the crosslink density did not last as the sample aged. The aged 25% reduced and 75% reduced samples had a comparable ice adhesion strength to the aged fully

crosslinked sample. It should also be noted that the 75% reduced sample no longer felt tacky after aging and that it is possible that the low molecular weight chains were removed by the hypochlorous acid. This might also help explain the large increase in ice adhesion strength for the aged 75% reduced samples. The hardness of the aged samples could not be determined because they were too thin to get an accurate hardness reading. Thus, it is unknown at present whether the stiffness of the samples changed during the aging process. The 50% reduced sample exhibited the lowest ice adhesion after aging and seemed far better than the 75% reduced and 25% reduced samples. However, the large scatter in the mass lost data suggest that the samples were not aged consistently from sample to sample. Thus, the conclusion from this data is that the ice adhesion strength will rapidly increase as the sample ages, especially for the low crosslinked samples.

Chapter Five: Summary and Conclusions

Summary

The FEM models showed that the ice adhesion test, similar in design to the Ling et al. [21] test apparatus, exhibits several critical flaws. The failure to remove the mold before performing an ice adhesion test will cause the vertical displacements to increase, which in turn will cause the normal stresses at the ice/substrate interface to increase. The piston position will also negatively impact the vertical displacements. The substrate thickness also affects the test, with the vertical displacements and normal stresses at the edges increasing as the substrate thickness increases. Furthermore, the stiffness of the substrate will affect all displacements and stresses at the interface, with softer materials deforming more than stiffer ones.

The experiments verified the FEM models for the mold and substrate thickness effects. The presence of the molds showed to be detrimental to the ice adhesion test and resulted in lower reported values for the ice adhesion strength. The results are in agreement with the FEM models because higher vertical displacements should result in higher normal stresses and lower apparent ice adhesion strengths. The substrate thickness test was also in agreement with the FEM models and showed that the ice adhesion strength decreased as the substrate thickness increased.

The experiments on partially crosslinked and aged PDMS samples showed that crosslink density does affect the ice adhesion strength, but the ice adhesion strength will rapidly increase as the samples age. The ice adhesion strength decreased as the PDMS crosslink density were lowered. This may be due to changing stiffnesses or to pooling of low molecular chains at the surface. However, the ice adhesion strength of the samples increased as they aged regardless of crosslink density, and low crosslink samples tended to be the most affected by aging.

Conclusion

The testing methods for the ice adhesion strength determination, investigated in this research, can be improved through several ways. First, any mold used to form the ice should be removed before commencing the ice adhesion test. The piston should also be positioned close to the base of the ice but not too close to drag against the sample. Finally, soft substrate samples of various thicknesses should be used to correct for any variations in the ice adhesion strength caused by the thickness effect. The ice cube adhesion test still has problems though, especially for softer materials. Materials like PDMS will deform regardless of the piston position and result in significant normal stresses to the ice/PDMS interfaces. Thus, the failure of the interface will be a mixed mode instead of pure shear. However, the modeling suggests that minimizing the sample thickness will reduce the undesirable normal deformation in softer materials.

The ice adhesion testing of varying crosslinked PDMS shows that the density does affect ice adhesion strength and aging of the PDMS samples revealed that lowering the cross-linked density will result in the faster loss of ice-phobic properties. Thus, lowering the crosslink density of PDMS is not an adequate method for producing long lasting extremely ice-phobic materials.

Work Cited

- [1] Lv, J., Song, Y., Jiang, L. & Wang, J. Bio-inspired strategies for anti-icing. *ACS Nano* 8, 3152–3169 (2014).
- [2] Ling, E. J. Y., Uong, V., Renault-Crispo, J. S., Kietzig, A. M. & Servio, P. Reducing Ice adhesion on Nonsmooth Metallic Surfaces: Wettability and Topography Effects. *ACS Appl. Mater. Interfaces* 8, 8789–8800 (2016).
- [3] Beemer, D. L., Wang, W. & Kota, A. K. Durable gels with ultra-low adhesion to ice. *J. Mater. Chem. A* 4, 18253–18258 (2016).
- [4] Golovin, K., Kobaku, S.P.R., Lee, D.H., Diloreto, E.T., J. M. Mabry, & Tuteja, A., Designing durable icephobic surfaces, no. March, (2016).
- [5] Davis, M. J., & McGregor, A., Importance of Failure Mode Identification.pdf, ISASI Aust. Saf. Semin. Canb erra, 1–12, (2010).
- [6] Cao, L., Jones, A. K., Sikka, V. K., Wu, J. & Gao, D. Anti-Icing superhydrophobic coatings. *Langmuir* 25, 12444–12448 (2009).
- [7] Kulinich, S. A. & Farzaneh, M. Ice adhesion on super-hydrophobic surfaces. *Appl. Surf. Sci.* 255, 8153–8157 (2009).
- [8] Kulinich, S. A. & Farzaneh, M. How wetting hysteresis influences ice adhesion strength on superhydrophobic surfaces. *Langmuir* 25, 8854–8856 (2009).

- [9] Zhu, X., Zhu, L., Chen, H., Yang, L. & Zhang, W. Applied Surface Science Micro-ball lens structure fabrication based on drop on demand printing the liquid mold. *Appl. Surf. Sci.* 361, 80–89 (2016).
- [10] <http://www.silicones.eu/science-research/chemistry/organomodified-siloxanes>, May, (2018).
- [11] <https://www.artmolds.com/condensation-addition-cured-silicone>, May, (2018).
- [12] Ozbay, S., Yuceel, C. & Erbil, H. Y. Improved Icephobic Properties on Surfaces with a Hydrophilic Lubricating Liquid. *ACS Appl. Mater. Interfaces* 7, 22067–22077 (2015).
- [13] Bharathidasan, T., Kumar, S. V., Bobji, M. S., Chakradhar, R. P. S. & Basu, B. J. Effect of wettability and surface roughness on ice-adhesion strength of hydrophilic, hydrophobic and superhydrophobic surfaces. *Appl. Surf. Sci.* 314, 241–250 (2014).
- [14] Haehnel, R.B., & Mulherin, N.D., The bond strength of an ice–solid interface loaded in shear, in: *Ice in Surface Waters, Proceedings of the 14th International Symposium on Ice*, 597–604, (1998).
- [15] Mulherin, N.D., Haehnel, R.B., & Jones, J.F., Toward developing a standard shear test for ice adhesion. *Proceedings, 8th International Workshop on Atmospheric Icing Structures, IWAIS*, (1998).
- [16] Arianpour, F., & Farzaneh, M., On Hydrophobic and Icephobic Properties of TiO₂ - Doped Silicon Rubber Coatings, vol. 1, no. 1, (2012).

- [17] Arianpour, F., Farzaneh, M. & Kulinich, S.A., Hydrophobic and ice-retarding properties of doped silicone rubber coatings Applied Surface Science Hydrophobic and ice-retarding properties of doped silicone rubber coatings. Appl. Surf. Sci. 265, 546–552 (2013).
- [18] Arianpour, F., Farzaneh, M., & Kulinich, S.A., Ice Adhesion and Hydrophobic Properties of Coatings Based on Doped RTV Silicone Rubber. (2009).
- [19] Jafari, R., Menini, R. & Farzaneh, M. Superhydrophobic and icephobic surfaces prepared by RF-sputtered polytetrafluoroethylene coatings. Appl. Surf. Sci. 257, 1540–1543 (2010).
- [20] Jafari, R., Momen, G. & Farzaneh, M. Durability enhancement of icephobic fluoropolymer film. J. Coatings Technol. Res. 13, 405–412 (2016).
- [21] Ling, E. J. Y., Uong, V., Renault-Crispo, J. S., Kietzig, A. M. & Servio, P. Reducing Ice Adhesion on Nonsmooth Metallic Surfaces: Wettability and Topography Effects. ACS Appl. Mater. Interfaces 8, 8789–8800 (2016).
- [22] Fu, Q. et al. Development of sol-gel icephobic coatings: Effect of surface roughness and surface energy. ACS Appl. Mater. Interfaces 6, 20685–20692 (2014).
- [23] Kim, P. et al. Liquid-infused nanostructured surfaces with extreme anti-ice and anti-frost performance. ACS Nano 6, 6569–6577 (2012).
- [24] <https://www.comsol.com/material-library>, May, (2018).
- [25] <https://www.plasticsintl.com/datasheets/Polycarbonate.pdf>, May, (2018).

[26] Petrovic, J.J. Mechanical properties of ice and snow. 8, 7–8 (2003).

[27] Bleszynski, M. Nanoengineering of Next Generation Silicone Rubbers Materials for Extreme Applications. (2018).

[28] Bleszynski, M. Aging Assessment of High Voltage Single Component Room Temperature Vulcanized Silicone Rubber (RTV-1) Subjected to Aqueous Salt. (2016).

Appendix – Acronyms and Symbols

A = Contact Area

°C = Degrees Celsius

cm = Centimeters

F = Force

hrs = hours

kPa = Kilo-Pascal

m = Mass of ice

mL = Milliliters

mm = Millimeters

N/s = Newtons per second

PDMS = Polydimethylsiloxane

r = Radius

RH = Relative Humidity

SHS = Super hydrophobic surfaces

SLIPS = slippery liquid-infused porous surfaces

t = thickness of substrate

W_{adh} = work of adhesion